Research Article

Open Access

Interaction of metallocene dichlorides with apo-human transferrin: A spectroscopic study and cytotoxic activity against human cancer cell lines

Abstract

Metallocene dichlorides ($Cp_2M(IV)Cl_2$) are the first class of small and hydrophobic organometallic compounds classified as anticancer agents against numerous cancer cell lines and tumors. In this study, the antiproliferative activities of Cp_2VCl_2, Cp_2NbCl_2, Cp_2HfCl_2 and Cp_2ZrCl_2 were assessed on two human cancer cell lines (HT-29 and MCF-7) using MTT assay. Spectroscopic studies were also conducted using these and other known metallocene dichlorides on apo-human transferrin (apo-hTf) at pH 7.4. UV-Vis and CD showed that their interaction with apo-hTf could induce conformational changes of its secondary structure during binding process. In fluorescence, a decrease in intensity of the emission peak was observed when the apo-hTf:$Cp_2M(IV)Cl_2$ complex is being formed, probably due to changes in the microenvironment of its tyrosine and tryptophan residues. Among all metallocene dichlorides studied, Cp_2VCl_2 has the strong ability to quench the intrinsic fluorescence of apo-hTf through a static quenching mechanism. The association constants for each protein-compound complex were also determined at different temperatures (296 K, 303 K, 310 K, and 317 K) based on fluorescence quenching results. Positive enthalpy changes (ΔH) and entropy changes (ΔS) as well as negative free energies (ΔG) suggest that hydrophobic interactions are the main intermolecular forces involved in the binding process, probably via an endothermic and spontaneous reaction mechanism. The distance, r, between donor (apo-hTf) and acceptor ($Cp_2M(IV)Cl_2$) obtained according to Forster's theory of non-radiation energy transfer suggest that the energy transfer from apo-hTf to $Cp_2M(IV)Cl_2$ occurs with high probability and distances obtained by FRET with high accuracy.

Keywords: apo human transferrin, metallocene dichlorides, anticancer activity, spectroscopic analysis, protein-ligand interactions

Volume 5 Issue 3 - 2020

Jorge R Güette Fernández, Xiomara Narváez Pita, Enrique Meléndez, Elsie I Parés Matos
Department of Chemistry, University of Puerto Rico, USA

Correspondence: Elsie I Parés Matos, Department of Chemistry, Faculty of Biochemistry and Biophysical Chemistry, University of Puerto Rico at Mayagüez, PO BOX 9000, Mayagüez, Puerto Rico, USA, Tel 17878324040, Fax 17872653849, Email elsie.paes@upr.edu

Received: April 23, 2020 | **Published:** July 31, 2020

Abbreviations: apo hTf, apo human transferrin; ATCC, American type culture collection; CD, circular dichroism; CDDP or $(NH_3)_2Pt(II)Cl_2$, *cis*-diamminedichloroplatinum (II); $Cp_2M(IV)Cl_2$, metallocene dichloride; CV, cyclic voltammetry; DMSO, dimethyl sulfoxide; EAT, ehrlich ascites tumour cells; FBS, fetal bovine serum; FRET, fluorescence resonance energy transfer; FTIR, Fourier-transform infrared spectroscopy; HT-29, human colorectal adenocarcinoma cell line; HTB, human tumor cell bank; IC_{50}, median inhibitory concentration; MCF-7, human breast adenocarcinoma cell line; MEM, minimum essential medium eagle; MRE, mean residue ellipticity; MTT, 3-(4,5-imethylthiazol-2-yl)-2,5-diphenyltetrazolium bromide; NMR, nuclear magnetic resonance; PBS, phosphate buffered saline; Tris-HCl, tris(hydroxymethyl)aminomethane hydrochloride; UV-Vis, ultraviolet-visible

Introduction

Metallocene dichlorides ($Cp_2M(IV)Cl_2$), also called *bis*(η^5-*cyclo*pentadienyl) metal dichlorides [(η^5-$C_5H_5)_2$-M(IV)-Cl_2], typically comprise of earlier transition metals in a formal (IV) oxidation state (Figure 1A) with electron configurations d^0 when M(IV)=Ti, Zr, Hf; d^1 when M(IV)=V, Nb, Ta; and d^2 when M(IV)=Mo, W.[1,2] Structurally, these *bis-cyclo*pentadienyl complexes are classified as bent metallocenes (Figure 1B), which have two η^5-*cyclo*pentadienyl (Cp) rings and two chlorine atoms coordinated to the metal atom.[3,4] In a clinical context,metallocene dichlorides represents the first class of small and hydrophobic organometallic compounds classified as anticancer agents with antiproliferative activity.[5,6] Several studies have established that their complexes exhibit high antitumor properties against numerous cell lines and in a wide range of murine and human tumors *in vitro* and *in vivo*[7,8] such as solid and fluid Ehrlich ascites tumors (EAT);[9–15] lymphoid leukemia L1210, lymphocytic leukemia P388 and L1210;[16] human breast adenocarcinoma (MCF-7);[17–19] human colorectal adenocarcinoma (HT-29) and Caco-2;[19–22] human testicular tumors (Tera-2 and NTera-2);[23] solid and fluid sarcoma 180;[24] solid B16 melanoma;[25] colon 38 adenocarcinoma;[25] Lewis lung carcinosarcoma;[26] mouse mammary tumor TA3Ha;[27,28] and several human colon adenocarcinomas (R85, CX-1 and C-Stg2),[29–32] human lung carcinomas (L182 and L261);[33] human breast adenocarcinoma (M3) and human stomach adenocarcinoma (M-Stg4);[34] and human renal carcinoma (KTCTL-1M, -2, -26A, -30 and -84) xenografted into athymic mice.[35]

Bent metallocenes, which have a *cis*-dichlorometal(IV) motif similar to *cis*-dichloroplatinum(II) of cisplatin (CDDP) (Figure 1C), are highly efficient and effective anticancer drugs considered as one of the most promising in the treatment of different types of cancer such as testicular, ovarian, head and neck, bladder, cervical, oesophageal and small cell lung cancer.[9,10,15,36] Cellular studies on $Cp_2M(IV)Cl_2$ have shown similar results to cisplatin, and have implicated DNA as the principal cellular target *in vivo* showing that cellular uptake and intracellular localization of several bent metallocenes were

Submit Manuscript | http://medcraveonline.com

©2020 Fernández et al. This is an open access article distributed under the terms of the Creative Commons Attribution License, which permits unrestricted use, distribution, and build upon your work non-commercially.

accumulated in significant amounts at nucleic acid-rich regions such as the nuclear heterochromatin, euchromatin and nucleolus of tumor cells,[44–46] inhibit cellular DNA biosynthesis,[47–49] cellular mitotic activities,[50–52] cellular RNA and protein biosynthesis[53–55] andcellular growth[14]. These results and its molecular structural similarities to cisplatin ($(NH_3)_2Pt(II)Cl_2$) led several authors to think that the anticancer activities of both $Cp_2M(IV)Cl_2$ and cisplatin compounds may have a similar DNA-binding mechanisms.[15,47,53] However, later studies showed that bent metallocenes have a mechanism of interaction with DNA completely different to that of cisplatin.[56–58] Among all metallocene dichlorides studied, titanocene dichloride (Cp_2TiCl_2) has been proved widely effective as a cytotoxic anticancer agent, which means that it can selectively kill cancer cells such as xenotransplanted human tumors of the colon, rectum, stomach, lung, breast and neck, and has been used in phase I and II clinical trials.[59–62]

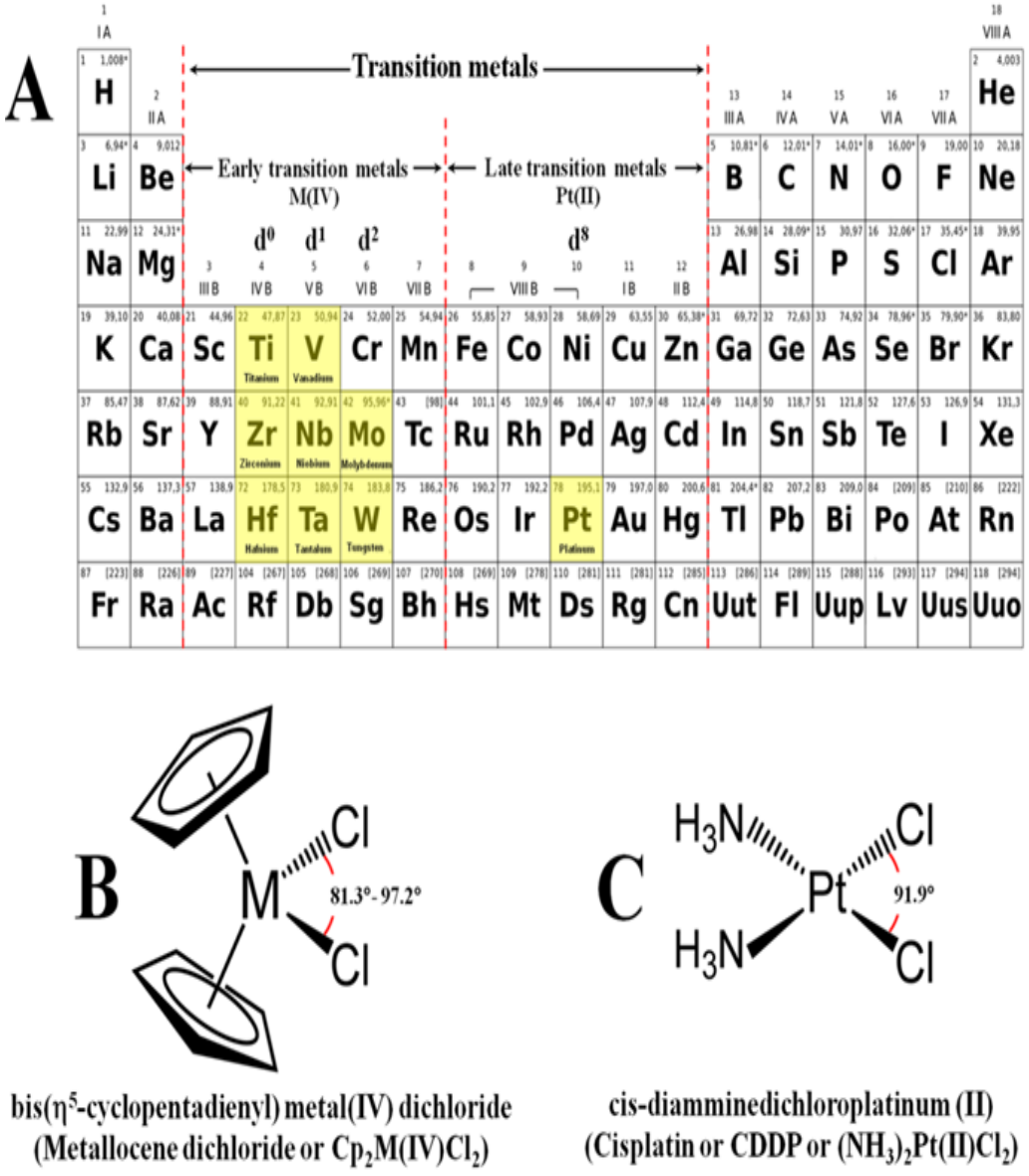

Figure 1 Transition metals as central atoms in antitumor agents. Some early and late transition metals (highlighted in yellow color) are known (A) to form $Cp_2M(IV)Cl_2$ and cisplatin, respectively. General representation of the molecular structure of a metallocene dichloride (B), where the angle $M_{(Cl-M-Cl)}$=Ti^{+4} (94.6°),[37] V^{+4} (87.1°),[38] Mo^{+4} (81.3°/82.0°),[39,40] Nb^{+4} (85.7°),[39] Zr^{+4} (97.2°),[39] W^{+4} (81.5°)[41] and Hf^{+4} (98.0°).[40] The molecular structure of cisplatin (C),where the Cl-Pt-Cl angle is 91.9°.[42,43]

Some amino acids and proteins have been considered as potential binding targets for these $Cp_2M(IV)Cl_2$. Several experimental and computational studies performed on $Cp_2M(IV)Cl_2$ with proteins including human transferrin (hTf),[41,63,64] human serum albumin (HSA),[19,65–66] protein kinase C (PKC),[55] topoisomerase II (TOPO II)[67] and ubiquitin (Ub)[68], have demonstrated that interaction with proteins and amino acids is needed to be considered in the transport and/or anticancer activity of $Cp_2M(IV)Cl_2$. Proteins are important chemical substances in our lives and the main target of all drugs in the organism. Human serum transferrin (hTf) is the most abundant serum protein, and it is responsible for the transport of both endogenous and exogenous compounds. Its utilization includes storage, transport, and homeostasis of iron in vertebrates.[69]

More recently and using vibrational and spectroscopic techniques, some research groups have reported interactions of different drugs with DNA, RNA and proteins using UV-Vis absorption, fluorescence, synchronous fluorescence, 3D fluorescence spectra, fourier transform infrared (FTIR), circular dichroism (CD), cyclic voltammetry (CV), and nuclear magnetic resonance (NMR) at physiological pH and molecular dockingstudies.[70,71] Spectroscopic studies on ligand-protein interaction are an important tool for providing crucial understanding for the design of novel anticancer drugs and to elucidate its possible modes of action and binding.[72] As a result, the spectroscopic information could also be used to target potential proteins for the transport of new drugs from bloodstream to the cell, due to the molecular recognition or interaction between the protein and ligand plays an important role in many biological processes which is essential for the treatment of different diseases,[73] especially using chemometric methods such as multivariate curve resolution-alternating least squares (MCR-ALS) method.[74,75] These studies have also reported a mode of action where hTf can play a key role in the transport of organometallic compounds such as $Cp_2M(IV)Cl_2$ for targeting cancer cells, and the strategy on how to deliver these therapeutic agents to the target cells.[76]

Nevertheless, neither of the reported experimental studies has a proposed mechanism of interaction between apo-hTf and $Cp_2M(IV)Cl_2$ in order to recognize which are the dominant intermolecular forces and conformational changes playing a role in the binding of $Cp_2M(IV)Cl_2$ to apo-hTf. In an attempt to do so, Güette et al. have recently reported the binding of $Cp_2M(IV)Cl_2$ complexes to apo-hTf *in silico*,[41] allowing to pinpoint which amino acid residues get engaged in mainly hydrophobic interactions with these metallic species. Thus, our main objective in this study is to determine the binding and thermodynamic parameters involved in interactions with seven $Cp_2M(IV)Cl_2$ complexes with apo-hTf using several spectroscopic techniques, but in conditions that may resemble the *in silico* studies, neither synergistic anion nor sodium chloride, only in a buffer solution. This study was performed for the current understanding of the potential mechanisms of action that organometallic compounds are employing during its binding to apo-hTf.

Materials and methods

Materials

Tris(hydroxymethyl) aminomethane hydrochloride(Tris-HCl) and dimethyl sulfoxide (DMSO) were purchased from Fisher Scientific. Double deionized distilled water was autoclaved and used to prepare 20 mM or 2 mM Tris-HCl at pH 7.4, and PBS (137 mM NaCl, 2.7 mM KCl, 10 mM Na_2HPO_4, 2 mM KH_2PO_4, pH 7.4). Both solutions were sterilized using cellulose-acetate 0.2µm filters. All $Cp_2M(IV)Cl_2$ (M(IV) =Ti, V, Mo, Nb, Hf, Zr, W) and apo-hTf were purchased from Sigma-Aldrich and used without further purification. For spectroscopic studies, apo-hTf and $Cp_2M(IV)Cl_2$ were prepared in Tris-HCl and Tris-HCl with 2% DMSO, respectively.[20] Human colorectal adenocarcinoma cell line HT-29 (ATCC HTB-38), breast cancer cell line MCF-7 (ATCC HTB-22), FBS and antibiotic/antimycotic (penicillin/streptomycin) were purchased from American Type Culture Collection (ATCC). McCoy's 5A modified medium with 1.5 mM L-glutamine was purchased from Lonza Walkersville Inc. Minimum Essential Medium (MEM) with Eagle's salts, 1.5 mM L-glutamine and 2.2 g/L sodium bicarbonate, bovine insulin, 0.25% trypsin-EDTA (w/v), 3-(4,5-dimethylthiazol-2-yl)-2,5-diphenyltetrazolium bromide (MTT), isopropanol and Triton-X100 were purchased from Sigma-Aldrich. HT-29 cells were grown in McCoy's 5A medium with L-glutamine supplemented with 10% (v/v) FBS and 1% (v/v) antibiotic/antimycotic.[19] MCF-7 cells were grown in MEM and supplemented with 10% (v/v) FBS, 1% (v/v) antibiotic/antimycotic and 0.01 mg/mL bovine insulin.[68] Both culture media were adjusted to pH 7.4 and sterilized using cellulose-acetate 0.2µm filters. For cytotoxic studies, all metallocene dichloride and apo-hTf solutions were prepared using growth media with 5% DMSO.[17]

MTT assay against two human cancer cell lines: HT-29 and MCF-7

MTT assays were performed to determine cytotoxicity of $Cp_2M(IV)Cl_2$ on two different cell lines obtained from American Type Culture Collection (ATCC): human colorectal adenocarcinoma cell line, HT-29 (ATCC HTB-38) and human breast adenocarcinoma cell line, MCF-7 (ATCC HTB-22). HT-29 cells were cultured into T25 flasks containing McCoy's 5A modified medium with 1.5 mM L-glutamine, and supplemented with 10% (v/v) fetal bovine serum and 1% (v/v) antibiotic-antimycotic. MCF-7 cells were also cultured into T25s flask containing Minimum essential Eagle medium with Earle's salts, 1.5 mM L-glutamine and 2.2 g/L sodium bicarbonate, and supplemented with 10% (v/v) fetal bovine serum, 1% (v/v) antibiotic-antimycotic and 0.01 mg/mL bovine insulin. Both cancer cell lines were incubated at 37°C under an atmosphere of 5% CO_2/95% air.[19] Culture media was replaced every 24-72 h to maintain optimum culture conditions. Once the cells have reached 70-80% confluency, the media was removed, the cells were washed with phosphate buffered saline (PBS) and trypsinized with 1 mL of 0.25% (w/v) trypsin-EDTA, and incubated briefly at 37°C to ensure complete cell detachment. Subsequently, cells were resuspended in fresh media, counted using a hemocytometer and 100µL of re suspended cells were seeded at a density of 1.5×10^4 cells/well into 96-well tissue culture plates, and incubated for 24 h under an atmosphere of 5% CO_2/95% air at 37°C, prior to $Cp_2M(IV)Cl_2$ treatment.[17]

After 24 h, grown cells were treated with 25µL of different concentrations of $Cp_2M(IV)Cl_2$ dissolved in 5% DMSO/95% culture media per well, either in the presence or absence of apo-hTf. Positive and negative control tests were performed in the presence and absence of cells contained 5% DMSO/95% culture media, respectively.[20] After treatment with $Cp_2M(IV)Cl_2$ for 72 h at 37°C and under an atmosphere of 5% CO_2/95% air, an aliquot of 75µL of 2.67 mg/mL MTT dissolved in culture media was added to each well and further incubated for 2 h to carry out the reduction of MTT into a purple water-insoluble formazan by mitochondrial succinate dehydrogenase. The MTT-contained media was removed and, subsequently, the cells were briefly rinsed with 200µL of cold 1X PBS. Formazan crystals were dissolved with 200µL of 10% (v/v) Triton X-100 solution in isopropanol and the absorbance readings were measured at 570 nm with a background subtraction at 620 nm in an ATTC Microplate Reader at room temperature.[68] The median inhibitory concentration (IC_{50}) was calculated using a sigmoidal plotting performed in the GraphPad Prism 3.0 software. Each assay contains eight replicas and was performed in triplicates.[77]

Spectroscopic analysis

UV-Vis absorbance

Absorbance spectra of apo-hTf, $Cp_2M(IV)Cl_2$ and apo-hTf:$Cp_2M(IV)Cl_2$ complexes were recorded in a Varian Cary 50 Bio UV-Vis spectrophotometer over a wavelength range from 250 nm to 560 nm using a 1.0 cm quartz cuvette. One milliliter of 1.0×10^{-5} mol L^{-1} apo-hTf dissolved in 20 mM Tris-HCl buffer at pH 7.4 was titrated

with different amounts of 1.0×10^{-3} mol L^{-1} $Cp_2M(IV)Cl_2$ (5, 10, 15, 20, 25, 30, 40, 50, 75, 100, 125, 150, 175, 200, 250, 300, 350 and 400 µL) to analyze changes in absorbance readings while formation of the ligand-protein complexes. The final concentration of $Cp_2M(IV)Cl_2$ varied from 0.00 mol L^{-1} to 2.86×10^{-4} mol L^{-1}. A difference spectra was generated for each aliquot of $Cp_2M(IV)Cl_2$ added to apo-hTf and after subtraction of the baseline with 20 mM Tris-HCl buffer at pH 7.4, either alone or with equal amount of DMSO at room temperature.[78]

Fluorescence spectroscopy

Fluorescence spectra of apo-hTf and apo-hTf:$Cp_2M(IV)Cl_2$ complexes were recorded in a Shimadzu RF-5301 PC spectrofluorophotometer equipped with a 150 W xenon lamp and temperature controller. All apo-hTf:$Cp_2M(IV)Cl_2$ complexes were prepared in a 1.0 cm quartz cuvette and analyzed using an emission wavelength range from 290 nm to 500 nm, excitation wavelength of 280 nm, excitation width of 10 nm and emission width of 5 nm. The emission spectra were also recorded at 296 K, 303 K, 310 K and 317 K to observe the stability of complex formation with changes in temperature. The quantitative analysis was performed by fluorometric titration. One milliliter of 1.0×10^{-5} mol L^{-1} apo-hTf in 20 mM Tris-HCl buffer at pH 7.4 was titrated with different amounts of 1.0×10^{-3} mol L^{-1} $Cp_2M(IV)Cl_2$ (5, 10, 15, 20, 25, 50, 75, 100, 125, 150, 175, 200, 250, 300, 350 and 400 µL) and at the different temperatures. All titrations were performed in triplicate.[65] Fluorescence intensities of the quenching spectra were corrected on absorbances at the excitation and emission wavelengths to decrease the inner filter effect, according to the following equation:

$$F_{cor} = F_{obs} \exp\left[\frac{A_{ex} + A_{em}}{2}\right]$$

where $F_{cor}$and F_{obs} are the corrected and observed fluorescence intensity, respectively, and A_{ex} and A_{em} are the absorbances at the excitation and emission wavelengths of $Cp_2M(IV)Cl_2$, respectively.[79]

Circular dichroism

Circular dichroism (CD) was used to find changes in the secondary structure of apo-hTf upon interaction with $Cp_2M(IV)Cl_2$ using far-UV (from 190 nm to 250 nm) and near-UV (from 250 nm to 300 nm) regions. CD spectra were carried out on a Jasco J-815 CD spectropolarimeter, equipped with a xenon lamp monochromatic linearly polarized. All CD measurements were done under a constant Nitrogen flow and using a 1.0 cm quartz cuvette. (+)-10-Camphorsulfonic acid was used for calibration of the spectropolarimeter following the manufacturer instructions. Six scans were accumulated and the spectral data was recorded in the range from 190 nm to 300 nm, with a scan speed of 100 nm/min. A volume of 2.5 mL of 4.0×10^{-7} mol L^{-1} apo-hTf in 2 mM Tris-HCl buffer at pH 7.4 was titrated with different amounts of 1.0×10^{-3} mol L^{-1} $Cp_2M(IV)Cl_2$ (0, 1, 2, 3, 4, 5 and 6 µL). The final concentration of $Cp_2M(IV)Cl_2$ varied from 0.0 mol L^{-1} to 2.4×10^{-6} mol L^{-1}. The baseline was run using 2 mM Tris-HCl buffer at pH 7.4, either alone or with equal amount of DMSO at room temperature.[68]

Data analysis

All the results were expressed as means ± standard deviation (SD). The cytotoxicity of metallocene dichlorides against MCF-7 and HT-29 was expressed as IC_{50}±SD and determined using GraphPad Prism, while cell viability vs log [$Cp_2M(IV)Cl_2$] plot was fitted to obtained the sigmoidal dose-response curves. UV-Vis absorption (at 280 nm and 360 nm) and fluorescence intensity (at 330 nm) data were plotted against [$Cp_2M(IV)Cl_2$] using linear regression analysis, and coefficient of determination (R^2) were reported as statistical measure that indicates the linear relationship between the evaluated variables. Binding constants and thermodynamic parameters were determined using different linear regression fit.

Results and discussion

Cytotoxicity studies of metallocene dichlorides against MCF-7 and HT-29

The antiproliferative activity of the metallocene dichlorideswas determined on colon cancer HT-29 and the hormone-dependent breast cancer MCF-7cell lines using the 3-(4,5-dimethylthiazol-2-yl)-2,5-diphenyltetrazolium bromide (MTT) cell viability assay, after a 72 h exposure.[80,81] Control experiments were run in 100% media and 5% DMSO/95% media. Both control experiments behaved identically within the experimental error, thus demonstrating that 5% DMSO in culture media does not have any cytotoxic effect on these cell lines, as reported previously.[17] Cytotoxicity values, expressed as IC_{50} for each $Cp_2M(IV)Cl_2$ against MCF-7 and HT-29,are summarized in Table 1 and their dose-response curves are shown in Figure 2. IC_{50} values were calculated using culture media as a control. Cp_2VCl_2 and Cp_2NbCl_2 exhibited antiproliferative effect on MCF-7 with an IC_{50} of 0.050 (±0.007) mM and 1.301 (±0.035) mM, respectively. Meanwhile, Cp_2HfCl_2 and Cp_2ZrCl_2 exhibited proliferative activity on MCF-7. Previous studies performed by Meléndez's group reported the antiproliferative activity of Cp_2TiCl_2 and Cp_2WCl_2 on MCF-7 with an IC_{50} of 0.570 (±0.005) mM[82] and 0.630 (±0.010) mM,[19] respectively. However, Cp_2MoCl_2 exhibited proliferative activity.[21,68] For the colon cancer HT-29 cell line, our cytotoxic data suggests that all $Cp_2M(IV)Cl_2$ have antiproliferative activity with an IC_{50} of 0.033 (±0.001) mM, 0.266 (±0.035) mM, 0.564 (±0.010) mM, and 0.774 (±0.020) mM for Cp_2VCl_2, Cp_2NbCl_2, Cp_2HfCl_2 and Cp_2ZrCl_2, respectively. Previous studies performed by Meléndez's group have also reported the antiproliferative activity of Cp_2TiCl_2, Cp_2WCl_2, Cp_2MoCl_2, and $(NH_3)_2Pt(II)Cl_2$on HT-29, with IC_{50} values of 0.413 (±0.002) mM,[82] 1.000 (±0.100) mM,[19] 2.600 (±0.300) mM,[21] and 0.066 (±0.002) mM,[77] respectively.

Table 1 Antiproliferative activities of seven $Cp_2M(IV)Cl_2$ and CDDP on human breast cancer MCF-7 and human colon cancer HT-29 cell lines, after 72 h of exposure. All experiments were performed in triplicate

Compound	IC50 (±SD), mM	
	MCF-7	HT-29
Cp^2VCl^2	0.050 (±0.007)	0.033 (±0.001)
Cp^2NbCl^2	1.301 (±0.035)	0.266 (±0.035)
Cp^2HfCl^2	Proliferative	0.564 (±0.010)
Cp^2ZrCl^2	Proliferative	0.774 (±0.020)
Cp^2TiCl^2	0.570 (±0.005)[82]	0.413 (±0.002)[82]
Cp^2WCl^2	0.630 (±0.010)[19]	1.000 (±0.100)[19]
Cp^2MoCl^2	Proliferative[21,68]	2.600 (±0.300)[21]
$(NH^3)^2PtCl^2$ (CDDP)	NR*	0.066 (±0.002)[77]
$(NH^3)^2PtCl^2$ (CDDP)	0.0020 (±0.0003)[83]	0.076 (±0.005)[85]
	0.0046 (±NR)[84]	0.023 (±NR)[84]

* NR = not reported

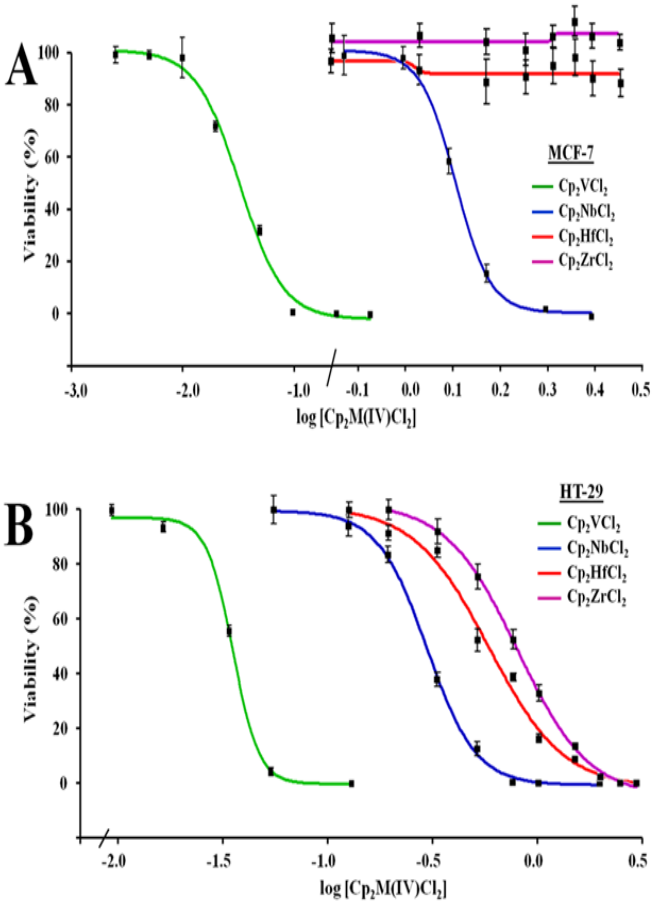

Figure 2 Dose-response curves of four metallocene dichlorides after their exposure for 72 h on two human breast cancer MCF-7 (A) and colon cancer HT-29 (B) cell lines.

Our recent cytotoxic studies suggest that HT-29 cells are more sensitive than MCF-7 cells when exposed to these metallocene dichlorides, with the exception ofCp_2WCl_2 and the standard chemodrug cisplatin ($(NH_3)_2Pt(II)Cl_2$). The results also suggest that after 72 h of exposure, Cp_2VCl_2 has more cytotoxic activity on both cancer cell lines. However, based on the cytotoxic studies performed by Schafer et al.,[83] and Mizumura et al.,[84] on MCF-7 cells, $(NH_3)_2Pt(II)Cl_2$ has an IC_{50} of 0.0020 mM and 0.0046 mM, respectively. Thus, $(NH_3)_2Pt(II)Cl_2$ is one order of magnitude more cytotoxic than Cp_2VCl_2. Otherwise, Cp_2VCl_2 has shown to be more cytotoxic on HT-29 cells than $(NH_3)_2Pt(II)Cl_2$, as shown by Narváez-Pita et al.,[77] and Leong et al.,[85] where an IC_{50} of 0.066 (±0.002) mM and 0.076 (±0.005) mM were reported, respectively. However, as seen in the Table 1, Cp_2VCl_2 has a level of cytotoxic activity similar to $(NH_3)_2Pt(II)Cl_2$ in agreement with the results reported by Mizumura et al.[84]

In summary, Cp_2VCl_2, Cp_2TiCl_2, Cp_2WCl_2, and Cp_2NbCl_2 have moderate to low anti-proliferative activity on MCF-7 cells (IC_{50} from 1.301 nm to 0.050 mM), but Cp_2HfCl_2, Cp_2ZrCl_2, and Cp_2MoCl_2 have no activity under similar experimental conditions. Meanwhile, Cp_2VCl_2 have a high antiproliferative activity, and Cp_2NbCl_2, Cp_2HfCl_2, Cp_2ZrCl_2, Cp_2TiCl_2, Cp_2WCl_2 and Cp_2MoCl_2 have moderate to very low antiproliferative activity on HT-29 cells (IC_{50} from 2.600 mM to 0.266 mM). Based on recent studies conducted by Meléndez's group, these results correlate well in terms of the solubility, aqueous stability and redox behavior of the $Cp_2M(IV)Cl_2$, suggesting that some metallocene dichlorides are quite stable at physiological pH whereas others can decompose in 3 h or less.[19,86] The aqueous stability of these metallocene dichlorides varies according to their Lewis acid character. Cp_2VCl_2 decomposes into $Cp_2V(OH)_2$, Cp_2NbCl_2 oxidizes to $Cp_2NbClOH$, and Cp_2MoCl_2 decomposes into $Cp_2Mo(H_2O)(OH)^+$ at physiological pH, meanwhile others such as $Cp_2M(IV)Cl_2$, M(IV)=Ti, Zr and Hf, undergo chloride loss and Cp pronoloysis, being Ti the most stable of the triad.[87,88] In addition, the oxidation potential can play an important role in the cytotoxic activity, because those metallocene dichlorides with higher oxidation potential are more stable to oxidation than those with low oxidation potential.[86] For example, the oxidation potential of Cp_2MoCl_2 is higher than of Cp_2WCl_2, suggesting that Cp_2MoCl_2 is less prone to oxidation than the tungstenocene counterpart. However, Cp_2WCl_2 has higher antiproliferative activity than Cp_2MoCl_2 on both MCF-7 and HT-29 cells.[19,86] The antiproliferative activity of these metallocene dichlorides also correlated well with the role played by the metal center and Cl–M–Cl angle with regard to the biological activity. Other studies have also concluded that the mechanism of tumor inhibition for the antineoplastic active and non-active metallocene dichlorides is inversely related to both an increased Cl…Cl non-bonding distance and Cl–M–Cl bond angle that may foreseeing the cancerostatic activity of these compounds.[41,89]

UV-Vis spectroscopy

UV-Vis spectroscopy is a simple, useful and relevant method used to explore the formation of protein-ligand complexes and to determine if protein conformational changes have occurred.[90,91] The absorption spectra of a protein can support fluorescence quenching experiments after a careful examination of the type of perturbation this protein is undergoing in the presence of ligands (or compounds). Dynamic quenching is mainly caused by collisions and affects only the excited state of the fluorophore and, therefore, no changes in absorption spectra are expected. Otherwise, a complex formation could also result in perturbation of the protein's absorption spectrum, thus suggesting a static quenching effect.[80,92] The binding effect of five $Cp_2M(IV)Cl_2$(M(IV)=V, Mo, W, Nb,and Ti) with apo-hTf was investigated using UV-Vis spectroscopy due to their promising antitumor activities. Figures 3&4 (as well as Figure S1 for Cp_2ZrCl_2, Cp_2HfCl_2 and $(NH_3)_2Pt(II)Cl_2$) show the effect caused by these compounds on the absorption spectra apo-hTf when assays were run at physiological pH and room temperature.

The absorption spectra of apo-hTf exhibited a strong absorption band at 280 nm characteristic of the $\pi \rightarrow \pi^*$ transition of the aromatic amino acid residues Trp, Tyr and Phe.[93] This band at 280 nm increases as the concentration of $Cp_2M(IV)Cl_2$ (M(IV) =V, Mo, W, Nb and Ti) increases as shown in Figures 3A, 3B, 3C, 4A and 4B, respectively. In addition to this hyperchromic effect, a slight red shift was also observed. These spectral changes might suggest that an interaction between apo-hTf and these metallocene dichlorides has occurred through a static quenching. A change in λ_{max} might be due to loosening and unfolding of the protein backbone. As a result, more changes in polarity around the Trp and/or Tyr microenvironment could occur due to changes in the secondary structure of apo-hTf and, hence, changes in hydrophobicity around these aromatic residues.[94,95] However, when Cp_2VCl_2, Cp_2MoCl_2, and Cp_2WCl_2 were added to apo-hTf, a broad new band appeared immediately at 361 nm and its intensity also increased with increasing amounts of these three compounds (Figures 3A,3B,3C, respectively). An equal effect was also observed with Cp_2TiCl_2, but the broadband appeared immediately around 340 nm (Figure 4B). This new band is similar to those observed for ligand to metal charge transfer (LMCT) transitions of metal(IV) with phenolate residues, and suggest to be attributed to the LMCT transition of M^{IV} with phenolate residues.[63] On the other hand, when Cp_2HfCl_2, Cp_2ZrCl_2 and $(NH_3)_2Pt(II)Cl_2$ were added to apo-hTf, the absorption band at 280 nm decreases with increasing concentration of these compounds, as can be seen in Figures S1A, S1B, and S1C, respectively. The results suggest a poor interaction between apo-hTf and these three compounds. The observed changes in absorbance readings of apo-hTf (in the presence of different concentrations of metallocene dichlorides) could suggest the occurrence of dynamic quenching interaction between Cp_2HfCl_2(or Cp_2ZrCl_2 or $(NH_3)_2Pt(II)Cl_2$) and apo-hTf.[80]

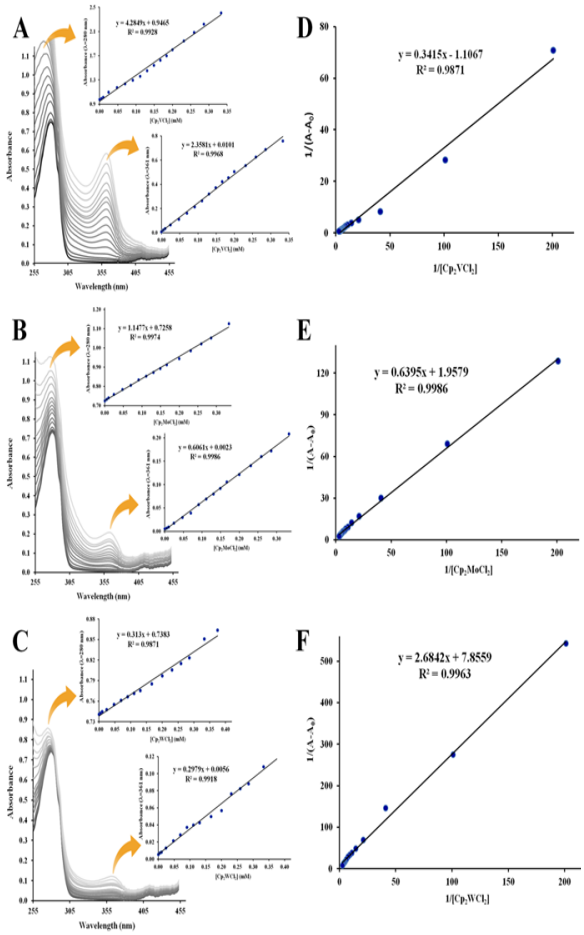

Figure 3 UV-Vis absorption spectra (T=298 K, pH=7.4) of 1.0×10^{-5} M apo-hTf in the presence of Cp_2VCl_2 (A), Cp_2MoCl_2 (B) and Cp_2WCl_2 (C).The insets show linear plot of absorbance vs [$Cp_2M(IV)Cl_2$] generated at 280 nm and 361 nm. Double reciprocal plots ($1/(A–A_0)$ vs $1/[Cp_2M(IV)Cl_2]$) of the Benesi and Hildebrand equation for Cp_2VCl_2 (D), Cp_2MoCl_2 (E) and Cp_2WCl_2 (F) were generated at280 nm.

Copyright: ©2020 Fernández et al.

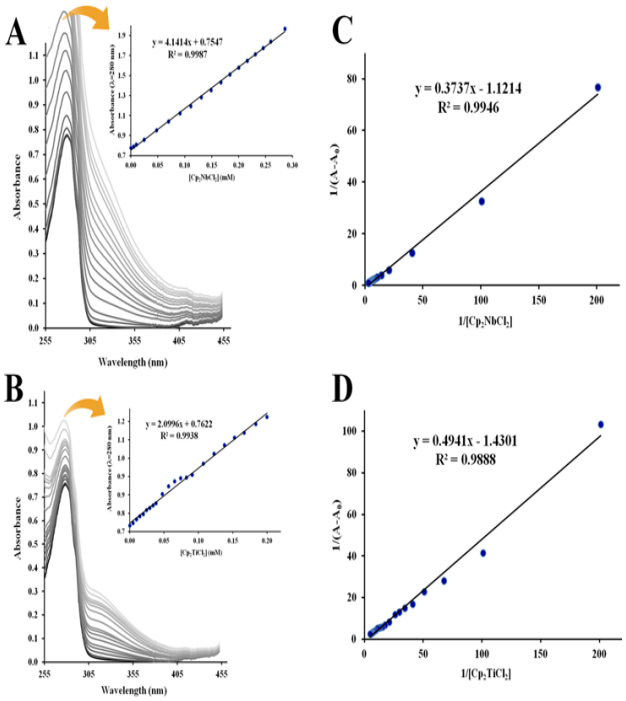

Figure 4 UV-Vis absorption spectra (*T*=298 K, pH=7.4) of 1.0×10^{-5} M apo-hTf in the presence of Cp_2NbCl_2 (A) and Cp_2TiCl_2 (B). The inset shows linear plot of absorbance vs $[Cp_2M(IV)Cl_2]$ at 280 nm. Double reciprocals plots ($1/(A–A_0)$ vs $1/[Cp_2M(IV)Cl_2]$) of the Benesi and Hildebrand equation for Cp_2NbCl_2 (C) and Cp_2TiCl_2 (D) were generated at280 nm.

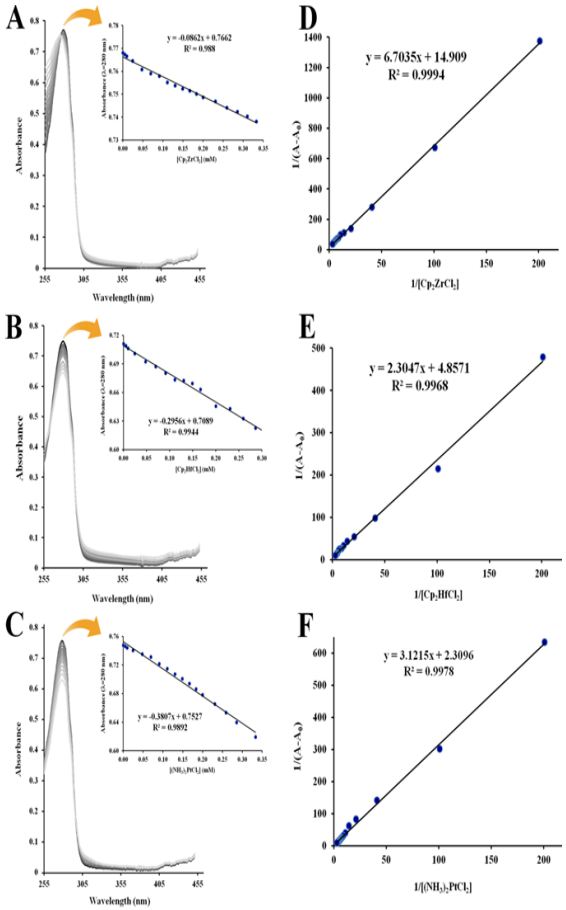

Figure S1 UV-Vis absorption spectra (*T*=298 K, pH=7.4) of 1.0×10^{-5} M apo-hTf in the presence of Cp_2ZrCl_2 (A), Cp_2HfCl_2 (B) and $(NH_3)_2Pt(II)Cl_2$ (C). The insets shows linear plot of absorbance vs $[Cp_2M(IV)Cl_2]$ (or $[(NH_3)_2Pt(II)Cl_2]$) generated at 280 nm. Double reciprocal plots ($1/(A–A_0)$ vs $1/[Cp_2M(IV)Cl_2]$ or $1/[(NH_3)_2Pt(II)Cl_2]$) of the Benesi and Hildebrand equation for Cp_2ZrCl_2 (D), Cp_2HfCl_2 (E) and $(NH_3)_2Pt(II)Cl_2$ (F) were generated at280 nm.

Citation: Fernández JRG, Pita XN, Meléndez E, et al. Interaction of metallocene dichlorides with apo-human transferrin: A spectroscopic study and cytotoxic activity against human cancer cell lines. *Int J Mol Biol Open Access*. 2020;5(3):79–109. DOI: 10.15406/ijmboa.2020.05.00136

Copyright: ©2020 Fernández et al.

The association constant (K_a) of each protein-ligand adduct could be determined by assuming that the interaction between a protein and its ligand occurs via a single complex and at a 1:1 ratio. For apo-hTf, the single complex formation could be shown as follows:

$$\text{apo-hTf} + Cp_2M(IV)Cl_2 \xrightleftharpoons{K_a} \text{apo-hTf:}Cp_2M(IV)Cl_2$$

It is also assumed that the Beer's law is followed,according to the following equation:

$$\frac{1}{A - A_o} = \frac{1}{K_a\left(A_\infty - A_O\right)}\frac{1}{\left[Cp_2M\left(IV\right)Cl_2\right]} + \frac{1}{A_\infty - A_o}$$

where A_0 and A are the absorption of apo-hTf in the absence and presence of $Cp_2M(IV)Cl_2$, respectively, and A_∞ is the final absorption of the ligated apo-hTf.[96] According to Stephanos et al. all these three variables could be obtained from the absorption data at 280 nm and 361 nm.[97]

The equilibrium of complex formation between apo-hTf and the metallocene dichlorides under study is given by the double reciprocal Benesi and Hildebrand equation.[96] Thus, K_a can be calculated from the intercept to the slope ratio of the linear double reciprocal plot of $1/(A–A_0)$versus $1/[Cp_2M(IV)Cl_2]$ based on the following equation:

$$K_a = \frac{Intercept}{Slope}$$

Figures 3, 4 and S2 show the linear double reciprocal plots of $1/(A–A_0)$ vs $1/[Cp_2M(IV)Cl_2]$. In summary, K_a was obtained for all metallocene dichlorides at 280 nm, but at 361 nm, it was only obtained for Cp_2VCl_2, Cp_2MoCl_2 and Cp_2WCl_2 (Table 2). At 280 nm, the K_a for Cp_2VCl_2 (Figure 3D), Cp_2MoCl_2 (Figure 3E) and Cp_2WCl_2 (Figure 3F) was 3.24×10^3 M^{-1}, 3.06×10^3 M^{-1} and 2.93×10^3 M^{-1}, respectively. Meanwhile at 361 nm, their K_a was 2.67×10^3 M^{-1}, 3.09×10^3 M^{-1} and 2.98×10^3 M^{-1}, respectively. For Cp_2NbCl_2 (Figure 4C) and Cp_2TiCl_2 (Figure 4D), the K_a(at 280 nm) was 3.00×10^3 M^{-1} and 2.89×10^3 M^{-1}, respectively. In addition, Cp_2ZrCl_2 (Figure S2A), Cp_2HfCl_2 (Figure S2B) and $(NH_3)_2Pt(II)Cl_2$ (Figure S2C) have a K_a (at 280 nm) of 2.22×10^3 M^{-1}, 2.11×10^3 M^{-1} and 7.4×10^2 M^{-1}, respectively. In general, all these K_a were found moderately large, in an order of magnitude of 10^3. However, the K_a for $(NH_3)_2Pt(II)Cl_2$ was considerably small, in an order of magnitude of 10^2.

Table 2 The association constants (K_a) of seven $Cp_2M(IV)Cl_2$ and DCCP,determined from calculations using the absorbance readings of apo-hTf at 280 nm and 361 nm

Compound	Association constants, Ka (10^3) (M^{-1})	
	280 nm	361 nm
Cp_2VCl_2	3.24	2.67
Cp_2MoCl_2	3.06	3.09
Cp_2WCl_2	2.93	2.98
Cp_2NbCl_2	3	–
Cp_2TiCl_2	2.89	–
Cp_2ZrCl_2	2.22	–
Cp_2HfCl_2	2.11	–
$(NH_3)_2Pt(II)Cl_2$	0.74	–

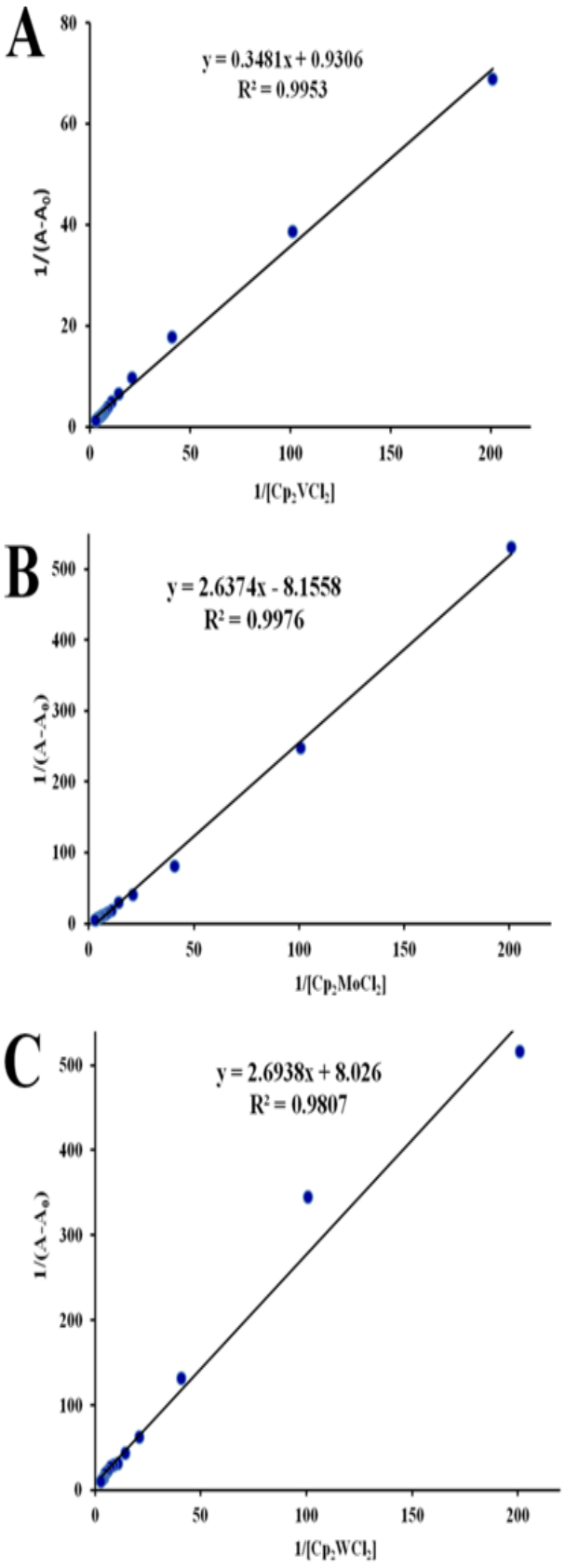

Figure S2 Double reciprocal plots ($1/(A–A_0)$ vs $1/[Cp_2M(IV)Cl_2]$) of the Benesi and Hildebrand equation for Cp_2VCl_2 (A), Cp_2MoCl_2 (B) and Cp_2WCl_2 (C) were generated at361 nm.

Fluorescence spectroscopy

Fluorescence spectroscopy is one of the most convenient and successful methods applied for the study of ligand-protein interactions. For biomacromolecules, fluorescence measurements provide information on ligand-protein interactions such as quenching mechanism, binding affinity between the ligand and protein for calculating binding constants, binding site for the ligand on a protein, nature of binding force for determining thermodynamic parameters and the intermolecular distance between the ligand and protein molecule.[90] Thus, the intrinsic fluorescence of proteins can provide considerable information regarding their structure and dynamics, and is often considered in the study of protein folding and association reactions. Consideration should also be taken to the fact that the intrinsic fluorescence of apo-hTf is very sensitive to its microenvironment. The intensity of the fluorescence of a substance can be affected or influenced by many factors, such as molecular rearrangements, collisions, complex formation, and energy transfer between two or more species, leading to what is called a fluorescence quenching spectrum.[96]

Fluorescence quenching studies of apo-hTf by seven $Cp_2M(IV)Cl_2$

When local surroundings of apo-hTf are slightly altered, its intrinsic fluorescence became significantly weakened, and factors such as protein conformational transition and biomolecule binding, among others, are responsible for this weakening. The fluorescence of apo-hTf emerges from its tryptophan, tyrosine, and phenylalanine residues.[98] Actually, the intrinsic fluorescence of apo-hTf came (almost completely) from tryptophan only, since phenylalanine has a very low quantum yield and the fluorescence of tyrosine is almost totally quenched if it is ionized or near an amino group, a carboxyl group, or even a tryptophan residue. This viewpoint was supported by the experimental observation of Sulkowska.[99] When a small molecule is bound to apo-hTf, changes in its intrinsic fluorescence intensity were induced by the microenvironment of the Trp/Tyr residues. The participation of tyrosine and tryptophan groups in those apo-hTf:$Cp_2M(IV)Cl_2$ complexes was assessed based on different excitation wavelengths. At a wavelength of 280 nm, both the tryptophanyl and tyrosyl residues in apo-hTf became excited.[98]

Quenching mechanism analysis

The quenching mechanism induced by the seven metallocene dichlorides was evaluated by temperature dependency of the fluorescence quenching, and their data were analyzed using the Stern-Volmer equation.[80]

$$\frac{F_o}{F} = 1 + K_{sv}\left[Q\right] = 1 + k_q\Gamma_o\left[Q\right]$$

where F_0 and F are the steady-state fluorescence intensities of apo-hTf in the absence and presence of the quencher ($Cp_2M(IV)Cl_2$), respectively, $[Q]$ is the concentration of the quencher, k_q is the biomolecular quenching rate constant, τ_0 is the average lifetime for biopolymer in the absence of the quencher, which is of the order of 1.0×10^{-8} s^{-1} for proteins, and K_{sv} is the Stern-Volmer quenching constant.[80] The quenching constant can be calculated using the following equation:

$$k_q = \frac{K_{sv}}{\Gamma_o}$$

Figures 5–7 and Figures S3–S7 show the fluorescence quenching spectra of apo-hTf after addition of different amounts of each metallocene dichloride and of $(NH_3)_2Pt(II)Cl_2$. The emission spectrum of apo-hTf, under the applied conditions, did show one emission band at 330 nm. In all cases, a decrease in the intensity of the emission band at 330 nm was observed with addition of the quencher. The results also suggest that the quenching effect on apo-hTf fluorescence intensity is dependent on the concentration of the ligand. For example, Cp_2VCl_2 and Cp_2NbCl_2 show a strong quenching effect on the apo-hTf intrinsic fluorescence intensity. Meanwhile, other $Cp_2M(IV)Cl_2$ (M(IV) =Mo, W, Ti, Zr, Hf), and even $(NH_3)_2Pt(II)Cl_2$, exhibits a moderate quenching effect on the apo-hTf intrinsic fluorescence intensity at both maximum emission wavelengths. All metallocene dichloridesalso induced a slight red shift of the emission band at 330 nm. The strong or moderate quenching and the slight red shift suggest that the microenvironment around both, tryptophanyl and tyrosyl residues, is changing as an indication that a molecular interaction have occurred and that an apo-hTf:$Cp_2M(IV)Cl_2$ complex has been formed.[96]

There are two different types of fluorescence quenching mechanisms known as dynamic and static quenching, depending on how the quencher molecule is interacting with the protein. Dynamic quenching depends on the diffusion of a quencher toward a fluorophore; therefore, they are in contact only through collision between fluorescent molecules and the quencher during the lifetime of the excited state. Static quenching is related to the formation of the complex and binding interactions between the fluorophore and quencher. One way to determine the quenching mechanism is by examining the behavior of the fluorophore in the presence of the quencher at different temperatures.[91] For that purpose, the fluorescence quenching spectra of apo-hTf were obtained at four different temperatures, and to elucidate a possible mechanism responsible for the quenching of the apo-hTf intrinsic fluorescence intensity, the Stern-Volmer equation was used for data analysis. Plots of F_0/F versus $[Q]$ are shown in Figures 5–7 and Figures S3–S7. Moreover, these plots exhibited fairly good linear relationships (R> 0.970) suggesting that a single quenching phenomenon, either static or dynamic quenching, have occurred during the formation of each apo-hTf:$Cp_2M(IV)Cl_2$ complex.[92] The slopes obtained from these plots correspond to the Stern-Volmer quenching constants (K_{sv}) and are summarized in Table 3. The dynamic quenching depends upon diffusion; hence, their quenching constants increase when the temperature increases. On the other hand, the static quenching is characterized by a decrease in their quenching constants as the temperature increases, thus promoting a decrease in the stability of the apo-hTf:$Cp_2M(IV)Cl_2$ complex. Another criterion used to classify the static quenching is k_q; a static quenching is observed when k_q is larger than the limiting diffusion collision quenching constant, K_D, of a biomolecule against different quenchers (2.0×10^{10} $M^{-1}s^{-1}$).[93]

Table 3 also shows the biomolecular quenching rate constant (k_q) for each apo-hTf:$Cp_2M(IV)Cl_2$ complex, obtained from the fluorescence quenching spectra at different temperatures. As shown in Table 3, all k_q were larger than K_D, independent of the apo-hTf:$Cp_2M(IV)Cl_2$ complex and, by following the maximum scatter collision mechanism, the static quenching process is mainly favorable. Furthermore, the K_{sv} and k_q of Cp_2VCl_2 and Cp_2NbCl_2 were at least one order of magnitude larger than for other $Cp_2M(IV)Cl_2$ (M(IV) = Mo, W, Ti, Zr and Hf). All K_{sv} and k_q were temperature dependent. For example, the trend

observed for K_{sv} and k_q was to increase as the temperature increases when $Cp_2M(IV)Cl_2$ (M(IV) = V, Nb, Mo, W and Ti), thus suggesting a dynamic quenching process, but for Cp_2ZrCl_2,$Cp_2HfCl_2$and $(NH_3)_2Pt(II)Cl_2$ the trend observed was to decrease as the temperature increases, thus suggesting a static quenching process (complex formation). These contradictory results raise the question about what type of interactions these metallocene dichlorides are really engaged with apo-hTf. At this point, we can only speculate that the apo-hTf:$Cp_2M(IV)Cl_2$ interaction is weak and labile, and prompted us to further use the fluorescence quenching spectra and K_{sv} to calculate their corresponding thermodynamic parameters.[19,68]

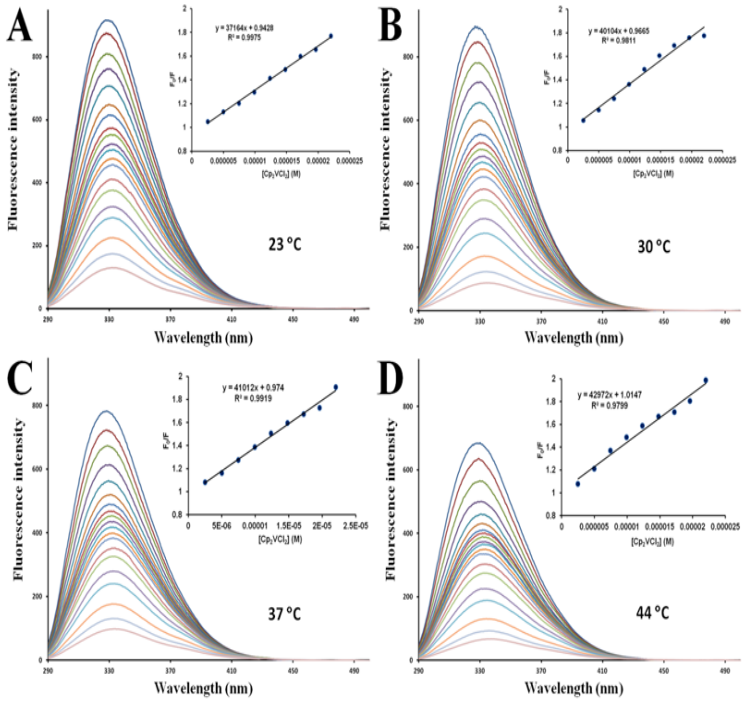

Figure 5 Fluorescence quenching of apo-hTf emission spectra with increasing amounts of Cp_2VCl_2 at296 K (A), 303 K (B), 310 K (C) and 317 K (D). A progressive decrease in the fluorescence intensity and a remarkable red shift was observed with addition of Cp_2VCl_2. The protein apo-hTf was excited at 280 nm, and its emission spectra was recorded in the range of 290 nm to 500 nm. Inset: Stern-Volmer plots of F_0/F versus [*Q*].

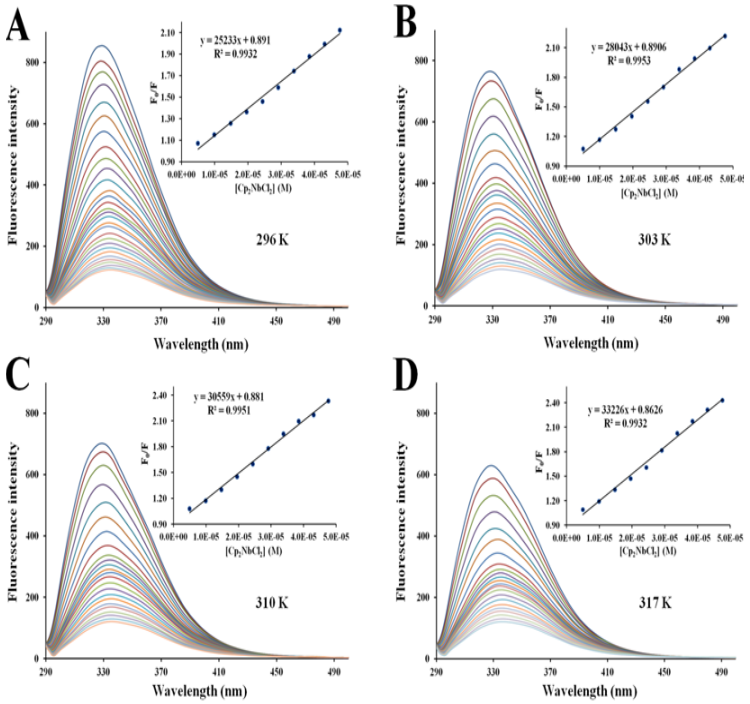

Figure 6 Fluorescence quenching of apo-hTf emission spectra with increasing amounts of Cp_2NbCl_2 at296 K (A), 303 K (B), 310 K (C) and 317 K (D). A progressive decrease in the fluorescence intensity and a remarkable red shift was observed with addition of Cp_2NbCl_2. The protein apo-hTf was excited at 280 nm, and its emission spectra was recorded in the range of 290 nm to 500 nm. Inset: Stern-Volmer plots of F_0/F versus [*Q*].

Copyright: ©2020 Fernández et al.

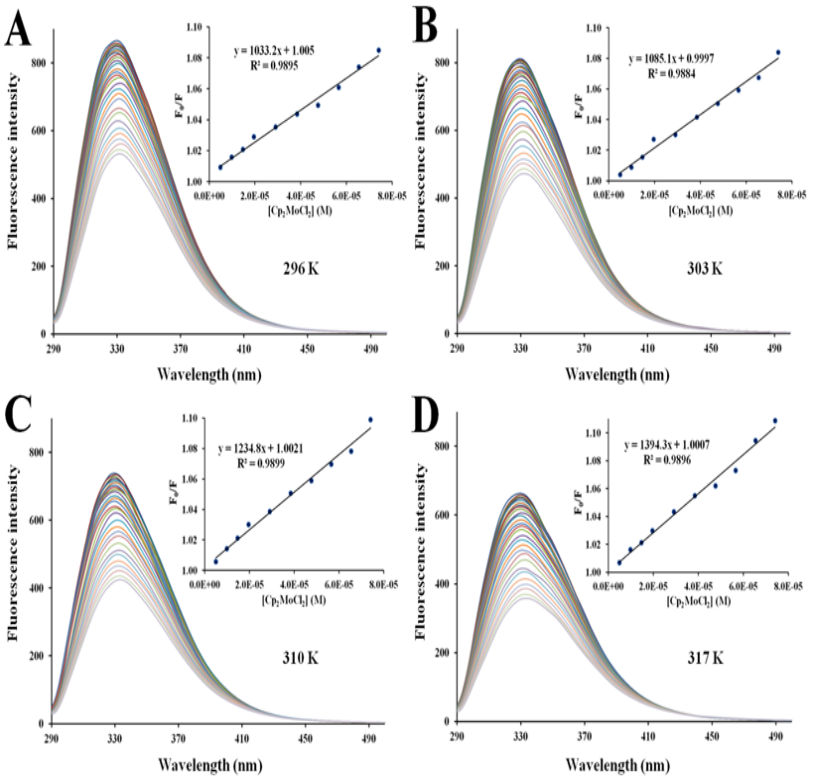

Figure 7 Fluorescence quenching of apo-hTf emission spectra with increasing amounts of Cp_2MoCl_2 at296 K (A), 303 K (B), 310 K (C) and 317 K (D). A progressive decrease in the fluorescence intensity and a remarkable red shift was observed with addition of Cp_2MoCl_2. The protein apo-hTf was excited at 280 nm, and its emission spectra was recorded in the range of 290 nm to 500 nm. Inset: Stern-Volmer plots of F_0/F versus [*Q*].

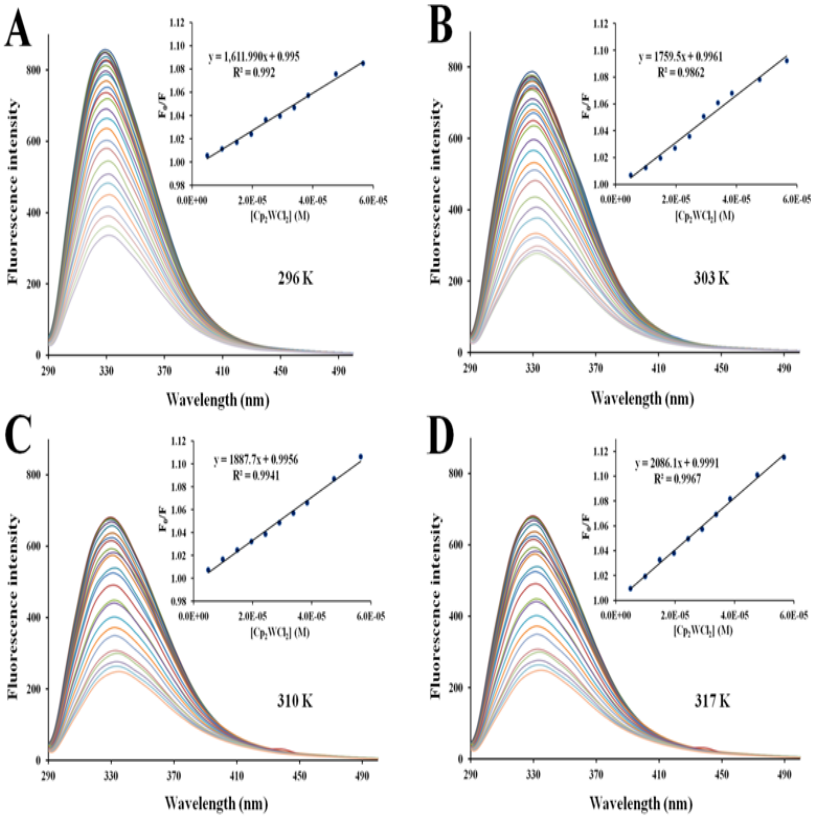

Figure S3 Fluorescence quenching emission spectra of apo-hTf with increasing amounts of Cp_2WCl_2 at296 K (A), 303 K (B), 310 K (C) and 317 K (D). A progressive decrease in the fluorescence intensity and remarkable red shift was observed while successive addition Cp_2WCl_2. The protein apo-hTf was excited at 280 nm and its emission spectra was recorded in the range of 290 nm to 500 nm. Inset: Stern-Volmer plots of F_0/F versus [*Q*].

Citation: Fernández JRG, Pita XN, Meléndez E, et al. Interaction of metallocene dichlorides with apo-human transferrin: A spectroscopic study and cytotoxic activity against human cancer cell lines. *Int J Mol Biol Open Access*. 2020;5(3):79–109. DOI: 10.15406/ijmboa.2020.05.00136

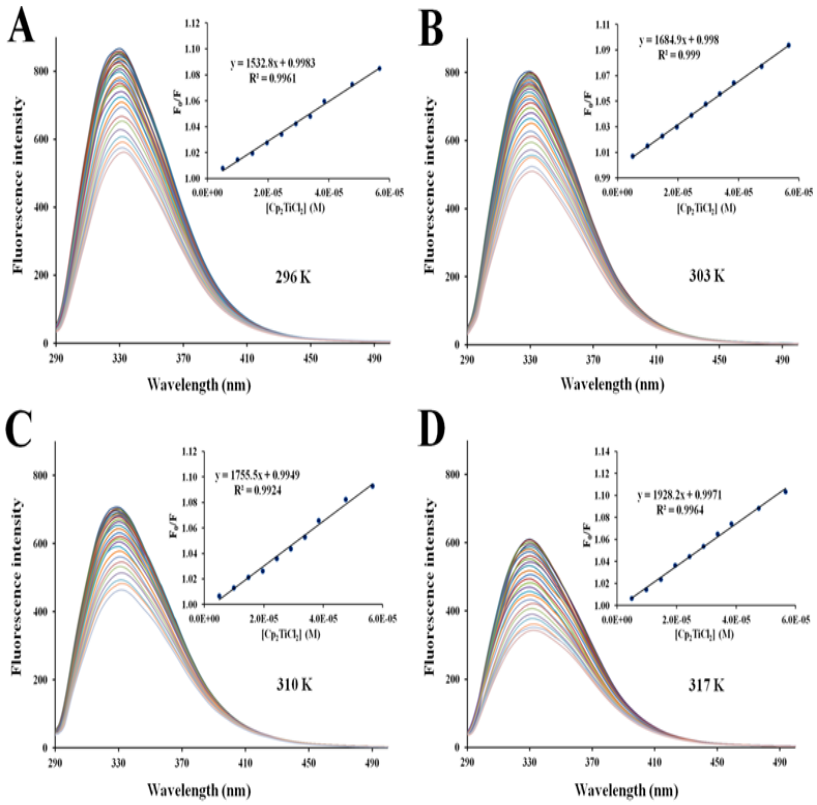

Figure S4 Fluorescence quenching of apo-hTf emission spectra with increasing amounts of Cp_2TiCl_2 at296 K (A), 303 K (B), 310 K (C) and 317 K (D). A progressive decrease in the fluorescence intensity and a remarkable red shift was observed with addition of Cp_2TiCl_2. The protein apo-hTf was excited at 280 nm and its emission spectra was recorded in the range of 290 nm to 500 nm. Inset: Stern-Volmer plots of F_0/F versus [*Q*].

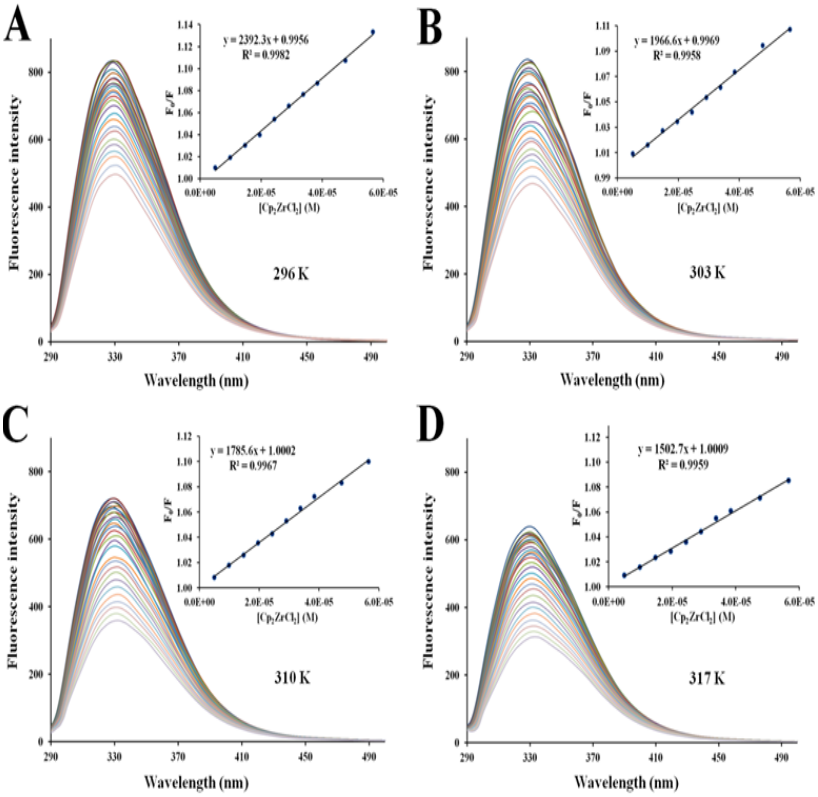

Figure S5 Fluorescence quenching emission spectra of apo-hTf with increasing amounts of Cp_2ZrCl_2 at 296 K (A), 303 K (B), 310 K (C) and 317 K (D). A progressive decrease in the fluorescence intensity and a remarkable red shift was observed with addition of Cp_2ZrCl_2. The protein apo-hTf was excited at 280 nm, and its emission spectra was recorded in the range of 290 nm to 500 nm. Inset: Stern-Volmer plots of F0/F versus [Q].

Citation: Fernández JRG, Pita XN, Meléndez E, et al. Interaction of metallocene dichlorides with apo-human transferrin: A spectroscopic study and cytotoxic activity against human cancer cell lines. *Int J Mol Biol Open Access*. 2020;5(3):79–109. DOI: 10.15406/ijmboa.2020.05.00136

Copyright: ©2020 Fernández et al.

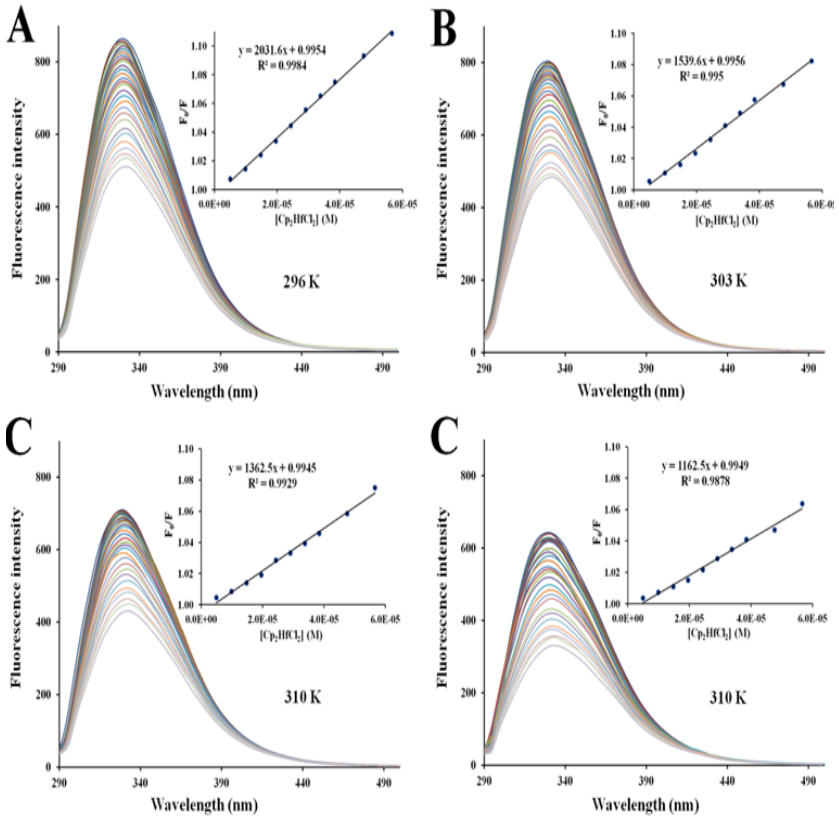

Figure S6 Fluorescence quenching emission spectra of apo-hTf with increasing amounts of Cp_2HfCl_2 at 296 K (A), 303 K (B), 310 K (C) and 317 K (D). A progressive decrease in the fluorescence intensity and a remarkable red shift was observed with addition of Cp_2HfCl_2. The protein apo-hTf was excited at 280 nm, and its emission spectra was recorded in the range of 290 nm to 500 nm. Inset: Stern-Volmer plots of F_0/F versus [*Q*].

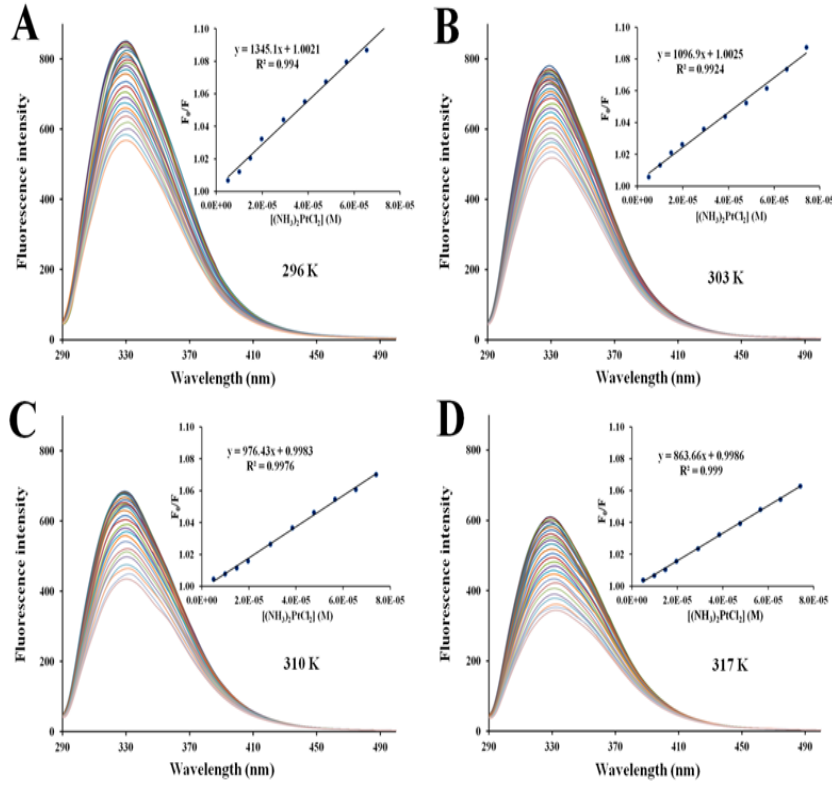

Figure S7 Fluorescence quenching emission spectra of apo-hTf with continuous addition of $(NH_3)_2Pt(II)Cl_2$ at296 K (A), 303 K (B), 310 K (C), and 317 K (D). A progressive decrease in fluorescence intensity and a remarkable red shift was observed with the addition of $(NH_3)_2Pt(II)Cl_2$. The protein was excited at 280 nm, and its emission spectra were recorded from 290 nm to 500 nm. Inset: Stern-Volmer plot of F_0/F versus [*Q*].

Citation: Fernández JRG, Pita XN, Meléndez E, et al. Interaction of metallocene dichlorides with apo-human transferrin: A spectroscopic study and cytotoxic activity against human cancer cell lines. *Int J Mol Biol Open Access*. 2020;5(3):79–109. DOI: 10.15406/ijmboa.2020.05.00136

Table 3 Stern-Volmer quenching constants K_{sv} and k_q, and the binding parameters n and K_a, for each apo-hTf: $Cp_2M(IV)Cl_2$complex formed at four different temperatures

Compound	Temperature (K)	K_{sv}(×10⁴) (M^{-1})	k_q(×10¹¹) ($M^{-1}s^{-1}$)	n	K_a(×10⁴)(M^{-1})
Cp_2VCl_2	296	3.564	35.64	1.23	44.44
	303	4.085	40.85	1.2	33.75
	310	4.26	42.6	1.16	24.05
	317	4.936	49.36	1.11	15.98
Cp_2NbCl_2	296	2.523	25.23	1.26	32.53
	303	2.804	28.04	1.27	40.81
	310	3.056	30.56	1.28	48.55
	317	3.323	33.23	1.29	56.23
Cp_2MoCl_2	296	0.151	1.51	1.26	1.93
	303	0.159	1.59	1.23	1.58
	310	0.181	1.81	1.19	1.21
	317	0.205	2.05	1.16	0.95
Cp_2WCl_2	296	0.161	1.61	1.16	0.78
	303	0.176	1.76	1.13	0.6
	310	0.189	1.89	1.08	0.42
	317	0.209	2.09	1.04	0.32
Cp_2TiCl_2	296	0.153	1.53	1.11	0.45
	303	0.168	1.68	1.09	0.41
	310	0.176	1.76	1.07	0.36
	317	0.193	1.93	1.05	0.31
Cp_2ZrCl_2	296	0.239	2.39	1.07	0.44
	303	0.197	1.97	1.03	0.26
	310	0.179	1.79	1.01	0.2
	317	0.15	1.5	1	0.16
Cp_2HfCl_2	296	0.197	1.97	1.15	0.89
	303	0.157	1.57	1.17	0.81
	310	0.136	1.36	1.18	0.75
	317	0.124	1.24	1.19	0.7
$(NH_3)_2Pt(II)Cl_2$	296	0.135	1.35	0.97	0.11
	303	0.11	1.1	1.01	0.12
	310	0.098	0.98	1.04	0.14
	317	0.086	0.86	1.07	0.16

Similar values of K_{sv} and k_q were also reported by Du et al. (K_{sv} = 3.0×10^4 M^{-1} and $k_q = 3.0\times10^{12}$ $M^{-1}s^{-1}$)[63] and Zhang et al. ($K_{sv} = 3.04\times10^4$ M^{-1} and k_q = 3.04×10^{12} $M^{-1}s^{-1}$)[64] for the apo-hTf:Cp_2VCl_2 complex, respectively. Both authors have concluded that the fluorescence quenching is a static quenching process. In addition, other studies conducted by Dominguez-Garcia et al.[19] and Narvaez-Pita et al.[68] evaluated the interactions of Cp_2WCl_2 with human serum albumin (HSA) and Cp_2MoCl_2 with ubiquitin (Ub), respectively. Their K_{sv} and k_q were found greater than K_D, thus showing the same order of magnitude as found for both dichloride metallocenes when studied with apo-hTf. These research groups also have found that K_{sv} and k_q can increase as temperature increases, thus suggesting a dynamic quenching process for these two specific protein-ligand complexes.

Evaluation of the binding constant and the binding site

For a static quenching process, the strength of the ligand-protein interaction is measured in terms of their binding affinity. When a ligand binds reversibly and independently to a set of equivalent

sites on a protein with different binding affinities, the quenching association constant (K_a) for the fluorophore,which is analogous to the association binding constant, and the number of binding sites (n) per protein molecule for the ligand-protein system can be obtained using the Modified Stern-Volmer equation:[91]

$$\log\left(\frac{F_o - F}{F}\right) = \log k_a + n \log\left[Q\right]$$

where F_0 and F are the steady-state fluorescence intensities of apo-hTf in the absence and presence of the quencher, respectively, and [Q] is the concentration of the quencher.

The binding parameters n and K_a were calculated for all $Cp_2M(IV)Cl_2$ and for $(NH_3)_2Pt(II)Cl_2$at a pH=7.4 and at four different temperatures, according to the plot of double logarithm regression curve of log[(F_0–F)/F] versus log[Q] as shown in Figure 8 and Figure S8. Moreover, the plots exhibited fairly good linear relationships (R> 0.970), suggesting that a static quenching process has occurred during formation of each apo-hTf:$Cp_2M(IV)Cl_2$ complex.[92] As shown in Table 3, the number of binding sites (n) obtained from the slope of the plot was found to be close to one, at all temperatures, thus suggesting that a single binding site is available, in agreement with Du et al.[63] and Zhang et al.[64] for the apo-hTf:Cp_2VCl_2 complex.

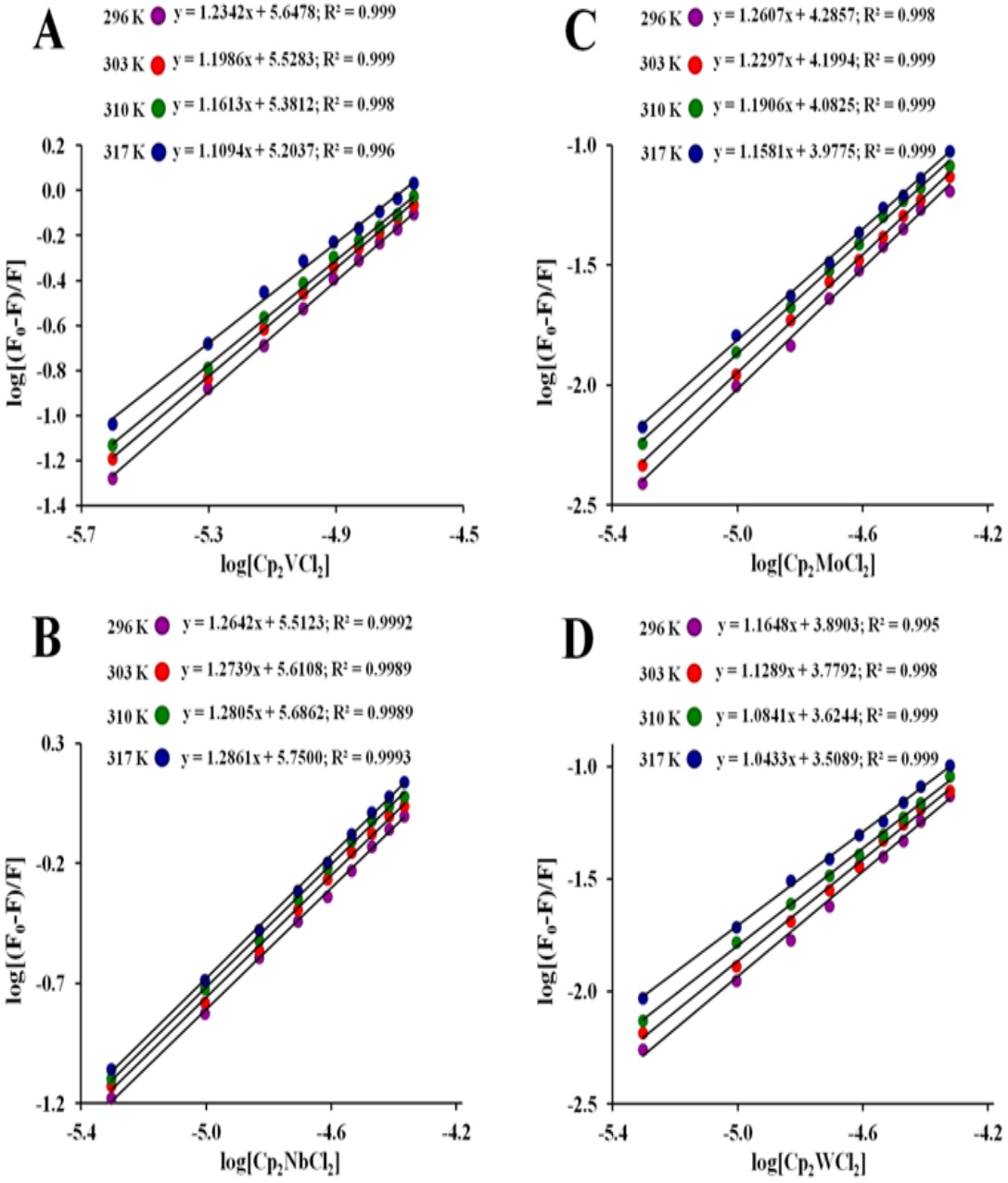

Figure 8 Modified Stern-Volmer plots of log [(F_0–F)/F] vs. log [Q]for the apo-hTf:$Cp_2M(IV)Cl_2$ complex formation at pH 7.4 and at four different temperatures (296 K, 303 K, 310 K and 317 K). Metallocene dichlorides used herein are Cp_2VCl_2 (A), Cp_2NbCl_2 (B), Cp_2MoCl_2 (C), and Cp_2WCl_2 (D).

Copyright: ©2020 Fernández et al.

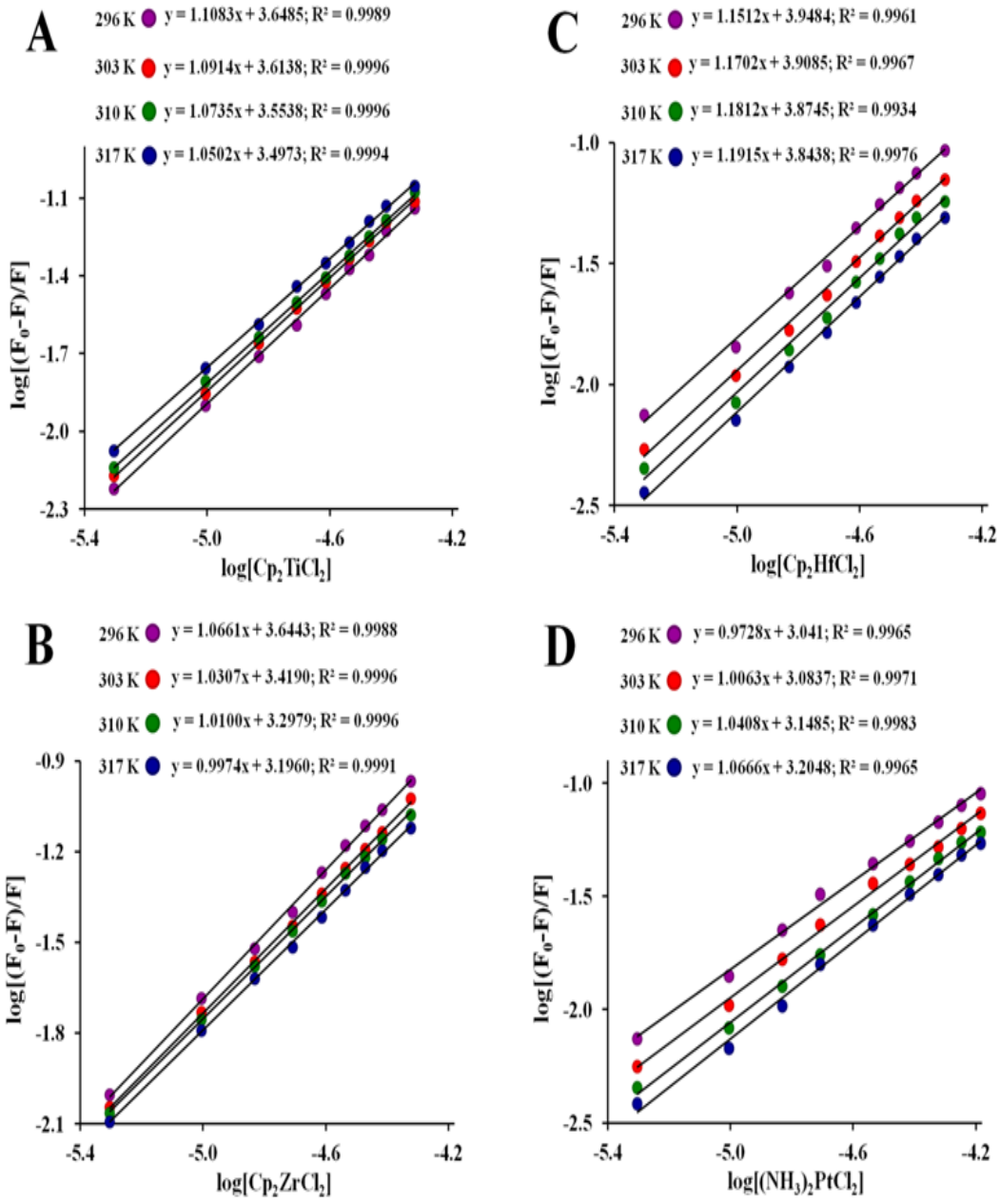

Figure S8 Modified Stern-Volmer plots of log [(F_0–F)/F] vs. log [Q]for the formation of four apo-hTf:$Cp_2M(IV)Cl_2$ complexes at pH 7.4 and at four different temperatures (296 K, 303 K, 310 K, and 317 K). Metallocene dichlorides used herein are Cp_2TiCl_2 (A), Cp_2ZrCl_2 (B), Cp_2HfCl_2 (C) and $(NH_3)_2Pt(II)Cl_2$ (D).

Based on each quenching association constant (K_a) obtained from the intercepts of these plots, it was found that for all metallocene dichloridesunder study, K_a is also temperature dependent. For $Cp_2M(IV)Cl_2$ (M(IV) = V, Mo, W, Ti, Zr and Hf), K_a decreases as the temperature increases, which suggests a reduction in the stability of the apo-hTf:$Cp_2M(IV)Cl_2$ complex when the temperature increases.[93] Meanwhile, for Cp_2NbCl_2 and $(NH_3)_2Pt(II)Cl_2$, K_a increases as the temperature increases. Additionally, the value of K_a for Cp_2VCl_2 and $Cp_2NbCl_2$is at least one order of magnitude larger (10^5 M^{-1}) than for Cp_2MoCl_2 (10^4 M^{-1}), and two orders of magnitude larger than for other $Cp_2M(IV)Cl_2$ (M(IV) =W, Ti, Zr, Hf) and for $(NH_3)_2Pt(II)Cl_2$ (10^3 M^{-1}), suggesting that apo-hTf has higher affinity for Cp_2VCl_2, Cp_2NbCl_2 and Cp_2MoCl_2 than for other metallocene dichlorides. As also shown in Table 3, the calculated binding constants for apo-hTf:$Cp_2M(IV)Cl_2$ (M(IV) =V, Nb and Mo) complexes suggest a moderated binding affinity with values within the range of 10^4 M^{-1} to 10^5 M^{-1} compared to other weak protein-ligand complexes (when M(IV) = W, Ti, Zr, Hf) with binding constants $\leq 10^3$ M^{-1} or for strong protein-ligand complexes with binding constants $\geq 10^6$ M^{-1}.[94] Dufour and Dangles[100] as well as Suryawanshi et al.,[95] among others, considered that most of these compounds (as ligands) can bind reversibly and exhibit moderate affinities to this protein. Thus, any binding between $Cp_2M(IV)Cl_2$ and apo-hTf could be considered as moderate, suggesting that a reversible apo-hTf:$Cp_2M(IV)Cl_2$ complex formation is possible, and that these metallocene dichlorides could be stored or carried by apo-hTf. Similar results for K_a were found by Du et al.[63] (K_a = 1.37x10^5 M^{-1}) and Zhang et al.[64] (K_a = 3.28x10^4 M^{-1}) when Cp_2VCl_2 was bound to apo-hTf.

However, both authors considered these K_a values much smaller than the binding constants obtained through UV-Vis (and by another methods) when other metals were bound to apo-hTf. However, the binding constants calculated from these fluorescence quenching methods are considered as an apparent association constant, which cannot be directly compared with the data found in the literature.

Thermodynamic parameters and binding forces

The temperature-dependent thermodynamic parameters for those interactions within the apo-hTf:$Cp_2M(IV)Cl_2$complex were calculated using the Van't Hoff equation:[90]

$$\ln k = -\frac{\Delta H^o}{RT} + \frac{\Delta S^o}{R}$$

where K is the binding constant at a corresponding temperature, ΔH^0 is the enthalpy change, ΔS^0 is the entropy change, R is the gas constant, and T is the absolute temperature. Therefore, the Gibbs free energy change (ΔG^0) at a corresponding temperature was subsequently derived from the following equation:[93]

$$\Delta G^o = -RT \ln k = \Delta H^o - T\Delta S^o$$

The results obtained for ΔH^0, ΔS^0 and ΔG^0 were then used to determine the intermolecular forces involved between $Cp_2M(IV)Cl_2$ and apo-hTf during complex formation. These intermolecular forces could be hydrophobic, hydrogen bonding, van der Waals or electrostatic. In general, Gibbs free energy change reflects the spontaneity of reaction, while ΔH^0 and ΔS^0 are the main quantities for judging the binding force.[95]

To pinpoint more the interactions involved during formation of the apo-hTf:$Cp_2M(IV)Cl_2$ complex, K_{sv} constants (at different temperatures) were also used to calculate the corresponding thermodynamic parameters governing these interactions using the Van't Hoff equation, since there is a clear dependence of these constants with the temperature, where it is a function of the intermolecular forces holding the complex together.[96] For all $Cp_2M(IV)Cl_2$ as well as for $(NH_3)_2Pt(II)Cl_2$, the three thermodynamic constants ΔH^0, ΔS^0 and ΔG^0 were calculated at pH 7.4, and at four different temperatures, according to the plot of regression curve of $\ln(K_{sv})$ versus 1/T as shown in Figure 9 and Figure S9. Moreover, these plots exhibited fairly good linear relationships (R >0.970) suggesting a clear dependence of K_{sv}, temperature and intermolecular forces, governing the formation of each apo-hTf:$Cp_2M(IV)Cl_2$ complex. The results shown in Table 4 suggest that these apo-hTf:$Cp_2M(IV)Cl_2$ complexes have been formed through a spontaneous ligand-protein interaction processes, because all ΔG^0 values were less than zero (negative ΔG^0). In addition, it seems that Cp_2VCl_2 (as well as Cp_2NbCl_2) can form a more stable complex with apo-hTf compared to other five $Cp_2M(IV)Cl_2$ (M(IV) =Mo, W, Ti, Zr and Hf) or even $(NH_3)_2Pt(II)Cl_2$.

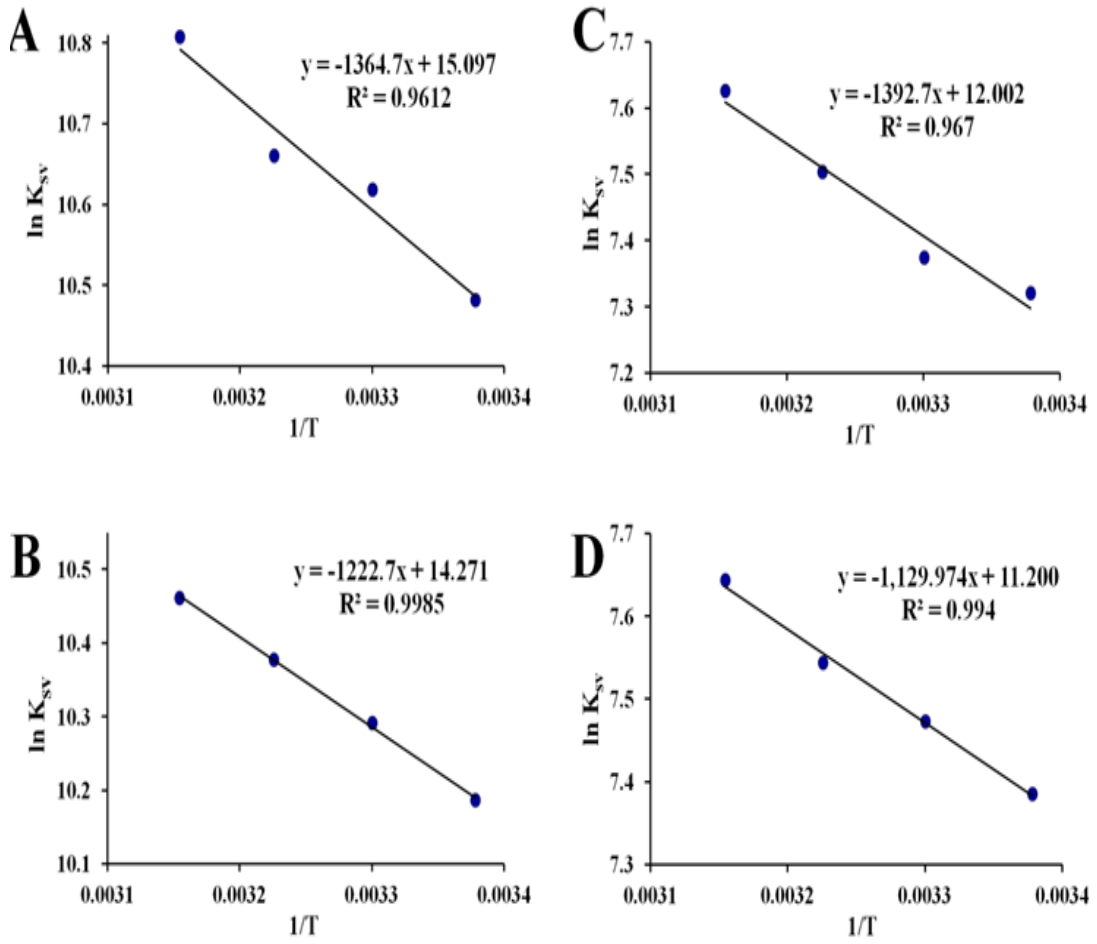

Figure 9 Van't Hoff plots for the interaction of apo-hTf with Cp_2VCl_2 (A), Cp_2NbCl_2 (B), Cp_2MoCl_2 (C) and Cp_2WCl_2 (D). All the experiments were performed at pH 7.4.

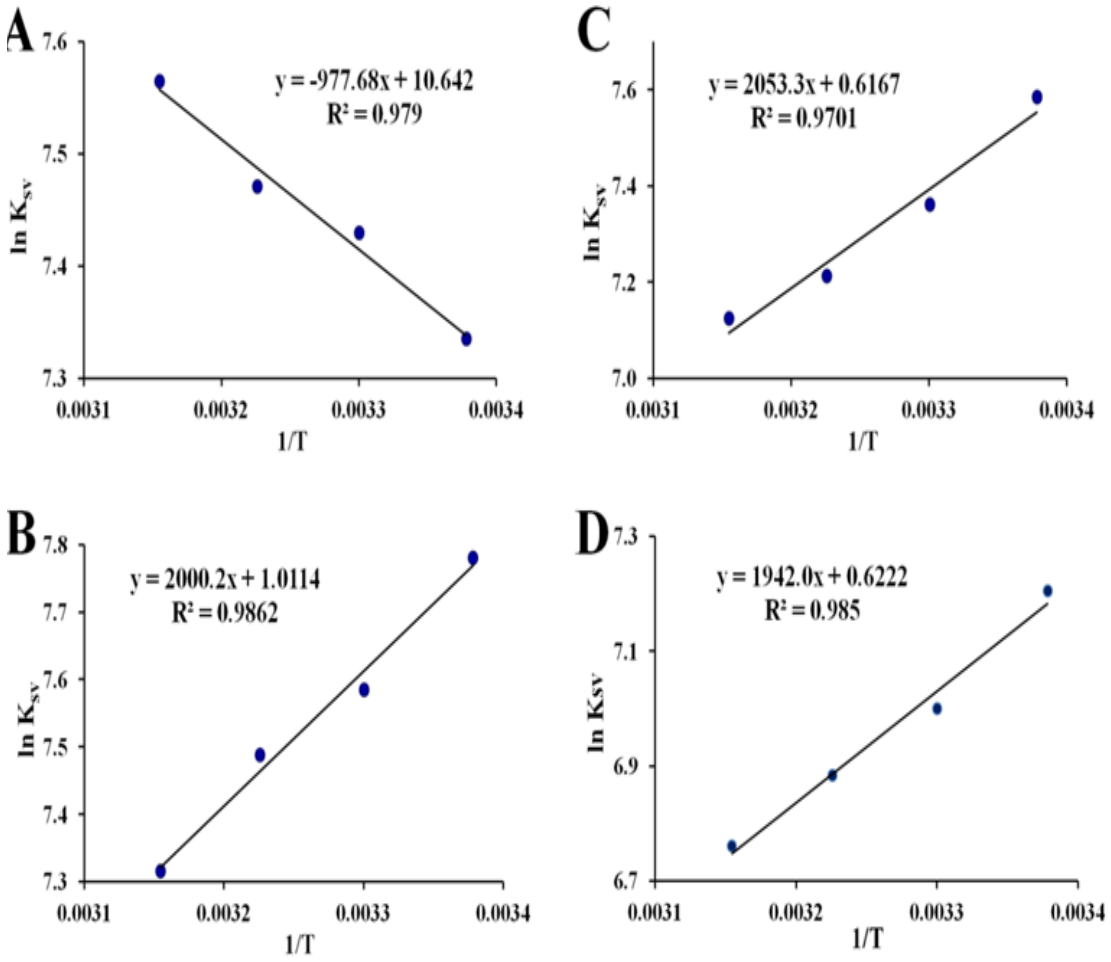

Figure S9 Van't Hoff plots for the interaction of apo-hTf with Cp_2TiCl_2 (A), Cp_2ZrCl_2 (B), Cp_2HfCl_2 (C) and $(NH_3)_2Pt(II)Cl_2$ (D) at pH 7.4.

Table 4 Thermodynamic parameters ΔH°, ΔS° and ΔG° calculated for each protein-compound complex generated with apo-hTf

Compound	Temperature (K)	ΔH° (kJ/mol)	ΔS° (J/mol K)	ΔG° (kJ/mol)
Cp_2VCl_2	296	11.35	125.52	–25.81
	303			–26.69
	310			–27.56
	317			–28.44
Cp_2NbCl_2	296	10.17	118.65	–24.95
	303			–25.79
	310			–26.62
	317			–27.45
Cp_2MoCl_2	296	11.58	99.78	–17.96
	303			–18.66
	310			–19.35
	317			–20.05
Cp_2WCl_2	296	9.39	93.12	–18.17
	303			–18.82
	310			–19.47
	317			–20.12

Table Continued...

Compound	Temperature (K)	ΔH° (kJ/mol)	ΔS° (J/mol K)	ΔG° (kJ/mol)
Cp_2TiCl_2	296	8.13	88.48	–18.06
	303			–18.68
	310			–19.30
	317			–19.92
Cp_2ZrCl_2	296	–16.63	8.41	–19.12
	303			–19.18
	310			–19.24
	317			–19.30
Cp_2HfCl_2	296	–17.07	5.13	–18.59
	303			–18.62
	310			–18.66
	317			–18.70
$(NH_3)_2Pt(II)Cl_2$	296	–16.15	5.17	–17.68
	303			–17.71
	310			–17.75
	317			–17.79

Ross and Subramanian have conceptualized a model for ligand binding to proteins based on the signs and magnitudes of the thermodynamic parameters and intermolecular forces contributing to the stability.[101] Their model proposes the following three conditions: $\Delta H^0 > 0$ and $\Delta S^0 > 0$ for hydrophobic interactions, $\Delta H^0 < 0$ and $\Delta S^0 < 0$ for van der Waals forces of attraction or hydrogen bonding, and $\Delta H^0 \sim 0$ (slightly positive or negative) and $\Delta S^0 > 0$ for electrostatic and ionic force interactions. Taking into account all of the above and the results from Table 4, the interactions between $Cp_2M(IV)Cl_2$ (M(IV) = V, Nb, Mo, W, Ti) and apo-hTf were mainly hydrophobic (both ΔH^0 and ΔS^0 were greater than zero) which suggest that formation of their apo-hTf:$Cp_2M(IV)Cl_2$ complexes were through an endothermic process, consistent with an increase of K_{sv} with temperature. Similar results were also reported by Dominguez García et al.,[19] and Narváez Pita et al.,[68] who found that hydrophobic interactions are mainly the intermolecular forces contributing to the stability between Cp_2WCl_2 and HSA as well as Cp_2MoCl_2 with Ub, respectively. On the other hand, Cp_2ZrCl_2, Cp_2HfCl_2 and $(NH_3)_2Pt(II)Cl_2$ show mainly hydrophobic interactions combined, most likely, with van der Waals interactions (dipole–dipole, dispersion), because their ΔH° were less than zero (negative ΔH^0) and their ΔS^0 were greater than zero (positive ΔS°), suggesting that formation of their complexes were through an exothermic process, consistent with a decrease in K_{sv} with an increase in temperature. Meanwhile, a positive ΔS° and a negative ΔH° suggests specificity through electrostatic interactions among ionic species in aqueous solution. However, this work should not be mainly attributed to electrostatic interactions since ΔS^0 was very small, almost zero for their binding interaction process. For all of these apo-hTf:$Cp_2M(IV)Cl_2$ complexes, the binding reaction mechanism were mainly supported by hydrophobic interactions because the principal contribution to ΔG^0 arose from ΔH^0 rather than from ΔS^0, thus making their binding process an enthalpy driven and, as a result, inducing hydrophobic interactions being supported by van der Waals interactions.[91] This is consistent with our previous *in silico* studies where we determined that those complexes formed with $Cp_2M(IV)Cl_2$ are engaged in hydrophobic interactions with apo-hTf's amino acid residues.[41]

Fluorescence resonance energy transfer (FRET) between apo-hTf and $Cp_2M(IV)Cl_2$

The fluorescence resonance energy transfer (FRET) technique was used to determine the energy transfer processes between apo-hTf (donor) and $Cp_2M(IV)Cl_2$ (acceptor) without emission of a photon and to measure the molecular distances in biological and macromolecular systems. FRET is a distance-dependent interaction between different electronic excited states of both donor and acceptor molecules. According to Forster's non-radiative energy transfer (FNRET) theory, the rate of energy transfer depends on three factors: (i) the distance between the donor and the acceptor, which should be < 7 nm, (ii) the relative orientation of the donor and acceptor dipoles, and (iii) the extent of overlap of the emission spectrum of the donor with the absorption spectrum of the acceptor.[102] The fluorescence emission spectra of 1.0×10^{-5} mol L^{-1} apo-hTf and the absorption spectra of 1.0×10^{-5} mol L^{-1} $Cp_2M(IV)Cl_2$ in 20 mM Tris-HCl buffer at pH 7.4 were obtained at room temperature in the wavelength range of 260 nm to 450 nm. The energy transfer effect is related not only to the distance r between the acceptor and donor, but also to the critical energy transfer distance R_0. The efficiency (E) of energy transfer between apo-hTf and $Cp_2M(IV)Cl_2$ was calculated, according to the Förster's equations:[103]

$$E = 1 - \frac{F}{F_o} = \frac{R_0^6}{R_0^6 + r^6}$$

where F_0 and F are the fluorescence intensities of apo-hTf in the absence and presence of $Cp_2M(IV)Cl_2$, respectively; r is the binding distance between the amino acid residues of the donor and acceptor in the binding sites; and R_0 is the Förster critical energy transfer distance when the efficiency (E) of energy transfer is 50% between the donor

and acceptor.The efficiency of the energy transfer E was calculated using the fluorescence intensities of apo-hTf (1.0×10^{-5} mol L^{-1}) without and with $Cp_2M(IV)Cl_2$ (1.0×10^{-5} mol L^{-1}) at room temperature, as shown in Table 5. R_0 was calculated from donor emission and acceptor absorption spectra using the following equation according to FNRET theory:[75]

$$R_0^6 = 8.8X10^{-25} k^2 n^{-4} \phi_D J$$

where k^2 is the spatial orientation factor related to the geometry of the donor-acceptor dipole, n is the refractive index of medium in the wavelength range where spectral overlap is significant, $\varnothing_D$ is the fluorescence quantum yield of the donor in the absence of acceptor, and J is the overlap integral of the emission spectrum of the donor and the absorption spectrum of the acceptor, which was calculated using the following equations:[90]

$$J = \frac{\sum F(\lambda)\varepsilon(\lambda)\lambda^4\Delta\lambda}{\sum F(\lambda)\Delta\lambda}$$

where$F(\lambda)$ is the fluorescence intensity of the fluorescent donor in the wavelength range from λ to $\lambda+\Delta\lambda$, $\varepsilon(\lambda)$ is the molar absorption coefficient of the acceptor at wavelength λ. J was calculated using a|e-UV-Vis-IR Spectral software 1.4.[104]J was evaluated by integrating, at a wavelength range from 260 nm to 450 nm, the overlap spectra of Figure10 and Figure S10, as shown in Table 5.

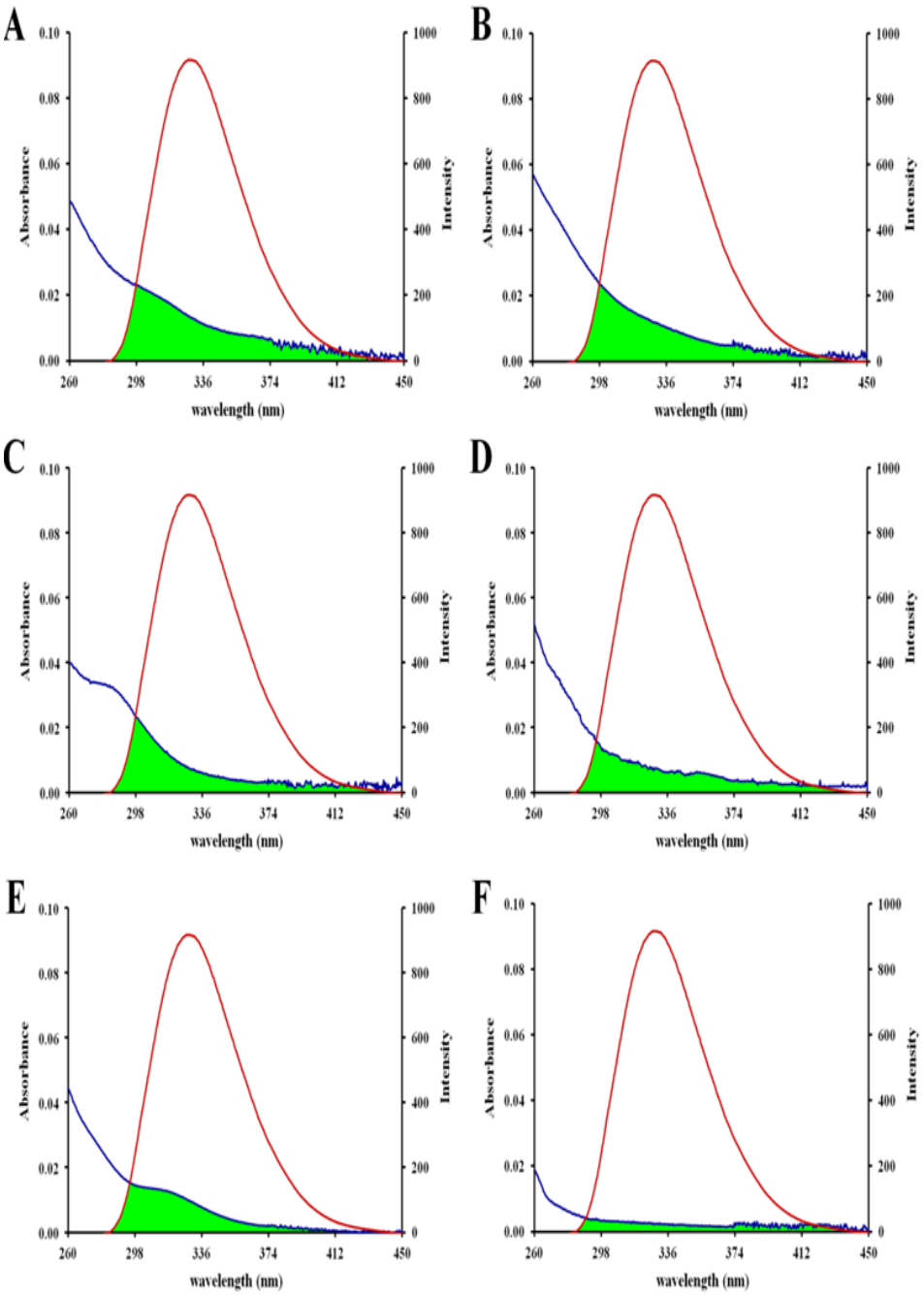

Figure 10 Overlap between fluorescence emission spectra of apo-hTf (1.0×10^{-5} mol L^{-1}) and UV-Vis absorption spectra of Cp_2VCl_2 (A), Cp_2NbCl_2 (B), Cp_2MoCl_2 (C), Cp_2WCl_2 (D), Cp_2TiCl_2 (E) and Cp_2HfCl_2 (F). All experiments were set at a final metallocene dichloride concentration of 1.0×10^{-5} mol L^{-1}.

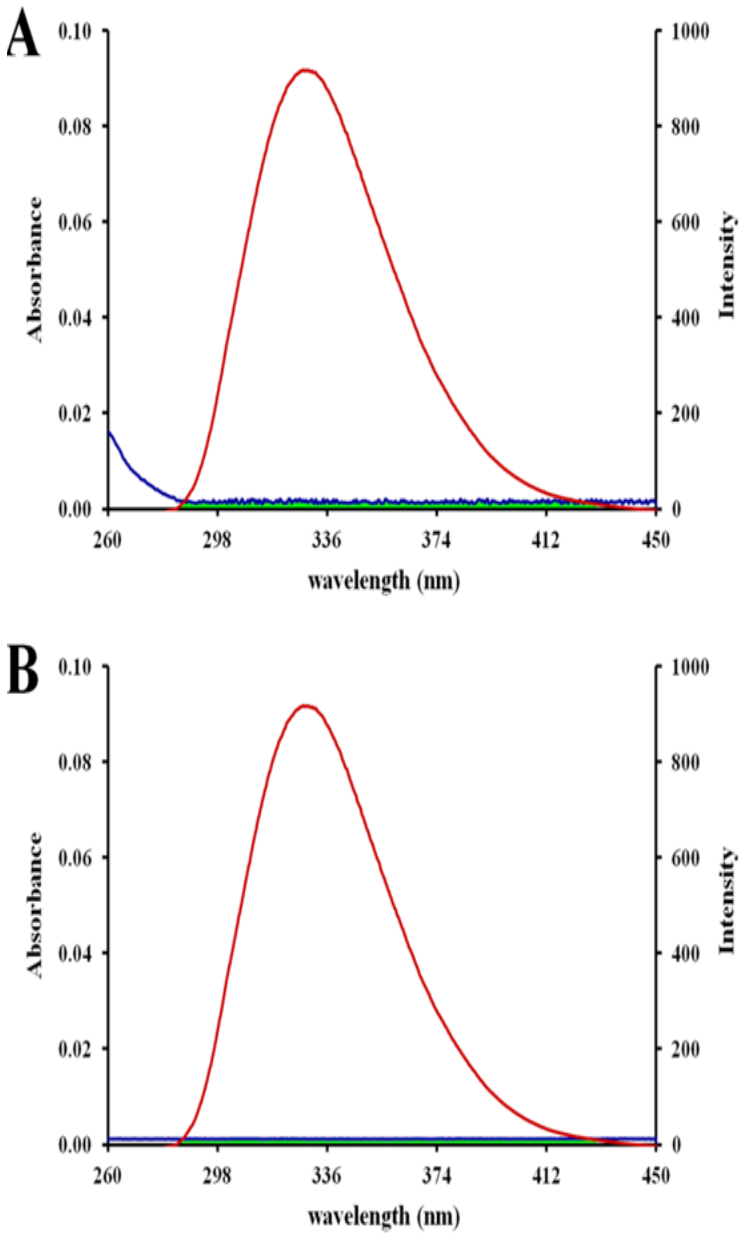

Figure S10 Spectral overlap of fluorescence emission spectra of 1.0×10^{-5} mol L^{-1} apo-hTf and UV-Vis absorption spectra of 1.0×10^{-5} mol L^{-1} Cp_2ZrCl_2 (A) and $(NH_3)_2Pt(II)Cl_2$ (B).

Table 5 Distance parameters calculated for those compounds that can bind apo-hTf

Compound	J ($cm^3\times L/mol$)	E	R_0 (nm)	r (nm)
Cp_2VCl_2	1.47×10-15	0.281	1.78	2.08
Cp_2NbCl_2	1.30×10-14	0.26	2.56	3.04
Cp_2MoCl_2	6.82×10-14	0.162	3.38	4.44
Cp_2WCl_2	3.99×10-13	0.15	4.53	6.05
Cp_2TiCl_2	7.48×10-13	0.144	5.03	6.77
Cp_2HfCl_2	5.03×10-12	0.131	6.91	9.47
Cp_2ZrCl_2	6.94×10-12	0.129	7.3	10.03
$(NH_3)_2Pt(II)Cl_2$	7.54×10-12	0.118	7.4	10.35

Citation: Fernández JRG, Pita XN, Meléndez E, et al. Interaction of metallocene dichlorides with apo-human transferrin: A spectroscopic study and cytotoxic activity against human cancer cell lines. *Int J Mol Biol Open Access.* 2020;5(3):79–109. DOI: 10.15406/ijmboa.2020.05.00136

The dipole orientation factor (k^2) is the least certain parameter that is used in the calculation of the critical transfer distance. Theoretically, k^2 can range from 0 to 4, and the extreme values require very rigid orientations. When both the donor and the acceptor tumble rapidly, and are free to assume any orientation, k^2 equals 2/3.[103] According to previous equations and using n= 1.336 and $\emptyset_D$ = 0.118 for apo-hTf,[105] the distance parameters R_0 and r can be obtained for each metallocene dichloride, as shown in Table 5.

The distance parameters R_0 and r were found to be between 1.78-7.40 nm, and between 2.08-10.35 nm, respectively. Average distances r between a donor (fluorophore) and acceptor (quencher) should satisfy the condition $0.5R_0 < r < 1.5R_0$ for a strong energy transfer in agreement to the FNRET theory.[102] For example, donor-acceptor distances r between apo-hTf and five of the $Cp_2M(IV)Cl_2$ (M(IV) = V, Nb, Mo, W and Ti) were found to be less than 7 nm, suggesting that the energy transfer between apo-hTf and these five metallocene dichlorides should occur with high probability, and by prediction of the FNRET theory, a static quenching interaction should also occur.[103,105] Meanwhile, the donor-acceptor distances r between apo-hTf and the last two $Cp_2M(IV)Cl_2$ (M(IV) =Hf and Zr) or between apo-hTf and $(NH_3)_2Pt(II)Cl_2$, were greater than 7 nm, suggesting that the energy transfer between apo-hTf and these two metallocene dichlorides, or between apo-hTf and $(NH_3)_2Pt(II)Cl_2$, should occur with low probability, and by prediction of the FNRET theory, a dynamic quenching interaction should also occur.[75,105] Additionally, the binding distance between the $Cp_2M(IV)Cl_2$ (M(IV) =V, Nb, Mo, W, Ti) and apo-hTf was found to be shorter than between $Cp_2M(IV)Cl_2$ (M(IV) =Hf, Zr) and apo-hTf, which suggest that the binding affinity between $Cp_2M(IV)Cl_2$ (when M(IV) =V, Nb, Mo, W, Ti) and apo-hTf is stronger than between $Cp_2M(IV)Cl_2$ (when M(IV) =Hf, Zr) and apo-hTf.[90] These findings are consistent with the results obtained from the UV-Vis and fluorescence spectra reported herein.

CD spectroscopy

Circular dichroism (CD) is an excellent, non-destructive and powerful technique for providing information about the secondary structure of a protein and its structural conformational changes when interacts with small molecules in solution. Far- and near-UV CD spectra can be used to characterize the secondary structure and side-chain environments of proteins, respectively.[68] The observed ellipticity in millidegrees, θ, were expressed in terms of the mean residue ellipticity (MRE), also called molar ellipticity [θ] in deg cm^2 $dmol^{-1}$, according to the following equation:[64]

$$\left[\theta\right] = \frac{observed\,\theta\left(m\deg\right)}{10C_p nl}$$

where C_p is the molar concentration of the protein, n is the number of amino acid residues in the protein and l is the path length (1.0 cm). The α-helical content of apo-hTf was calculated from the [θ] value at 208 nm using the following equation:[64]

$$\%\alpha - helix = \frac{\left[\theta\right]_{208} - 4000}{33000 - 4000} = \frac{\left[\theta\right]_{208} - 4000}{29000}$$

where $\left[\theta\right]_{208}$ are the experimental MRE values at 208 nm; 33,000 and 4,000 are the MRE values for a pure α-helix and pure β-sheet, and for a random coil conformation, respectively, at 208 nm. The β-sheet and random coil content of apo-hTf were calculated using the Raussens et al. method (CD-RRG).[106]

Figure 11 and Figure S11 show the far-UV CD spectra of apo-hTf in the absence and presence of different concentrations of $Cp_2M(IV)Cl_2$ in 2.0 mM Tris-HCl buffer at pH 7.4. The obtained far-UV CD spectra of native apo-hTf were consistent with those previously reported by Tomimatsu et al.,[107] Ali et al.,[108] and Amroabadi et al.,[96] The far-UV CD spectrum of apo-hTf (between 190 nm and 250 nm) shows the prevalence curve for a typical α-helix structure with a broad positive maximum around 193 nm and a negative minimum around 209 nm. The absorption within this region is mainly due to the peptide bond (amide groups) and are influenced by the geometries of the polypeptide backbone. There is a weak, but broad, n→π* transition centered around 209 nm and a more intense π→π* transition around 193 nm.[105]

After titration of $Cp_2M(IV)Cl_2$ (M(IV) =V, Nb, Mo and W), the far-UV CD spectra of apo-hTf showed significant changes in its absorption curve at both wavelengths 193 nm and 209 nm (Figure 11), when compared to the far-UV CD spectra of native apo-hTf. However, when apo-hTf was titrated with $Cp_2M(IV)Cl_2$ (M(IV) =Ti, Hf, Zr) and with $(NH_3)_2Pt(II)Cl_2$, the far-UV CD spectra were not disturbed (Figure S11A). As shown in Figure 11, a decrease in peak intensity (red insets) was observed at 193 nm and 209 nm, suggesting a strong conformational change of apo-hTf when titrated with $Cp_2M(IV)Cl_2$ (M(IV) =V, Nb, Mo and W). The results suggest that these metallocene dichlorides can induce changes on the protein secondary structure of apo-hTf, and even at very low concentration. Table 6 shows the percentages calculated from the obtained CD spectral data of the secondary structure elements in apo-hTf, in the presence and absence of $Cp_2M(IV)Cl_2$. In general, the percentage of α-helix decreases as the concentration of the metallocene dichloride increases, whereas the percentages of β-sheet and random coil increased. These changes were more notable when apo-hTf was titrated with $Cp_2M(IV)Cl_2$ (M(IV) =V, Nb, Mo and W) than with $Cp_2M(IV)Cl_2$(M(IV) =Ti, Hf, Zr) and $(NH_3)_2Pt(II)Cl_2$. The CD data suggest, in agreement with fluorescence studies, that somewhat changes in its secondary structure occur when apo-hTf is involved in interactions with these metallocene dichlorides. The black insets located in Figure 11 and Figure S11A show the relationship between the changes in mean residue molar ellipticity at 209 nm with respect to metallocene dichloride concentration. The results suggest that these metallocene dichlorides can induce a loss of the apo-hTf secondary structure upon binding, as a signal of complex formation.

The far-UV CD spectra of apo-hTf (in the absence of a metallocene dichloride) show a percentage of α-helix stretching from 29.0% to 30.2% and of β-sheet stretching from 17.3% to 18.1%. The results were similar to those reported by Amroabadi et al., where the CD spectral data of native apo-hTf was determined to be 30.2% for α-helix and 16.9% for β-sheet using the Chou and Fasman method.[96] On the other hand, Nishikawaalso obtained similar results (31% of α-helix and 18% of β-sheet) from the 3D structure of apo-hTf defined by crystallographic measurements.[109] However, Ali et al. reported an analysis of the far-UV CD spectrum of recombinant apo-hTf with the SELCON program, showing a well-defined secondary structure with an α-helix and β-sheet content of 41.5% and 28.4%, respectively.[108]

Near-UV CD spectrum of native apo-hTf (from 250 nm to 300 nm) shows different bands due to the aromatic amino acid residues within the protein. This spectral range also gives information on short-range interactions of the aromatic side chains of apo-hTf with other optically active groups of the protein, including other aromatic side chains.[96] Changes in position or interactions among the aromatic groups may imply changes in CD spectra recorded in the range of 250 nm to 300 nm. Signals at a wavelength range from 250 nm to 270 nm are attributed to phenylalanine, from 270 nm to 290 nm are attributed to tyrosine, and those from 290 nm to 300 nm are attributed to tryptophan.[105] These bands regularly decrease or increase with increasing concentration of metallocene dichloride, suggesting that the interaction apo-hTf with these compounds partially disrupts the anisotropic environment of the aromatic residues (Figure 12 & Figure S12).

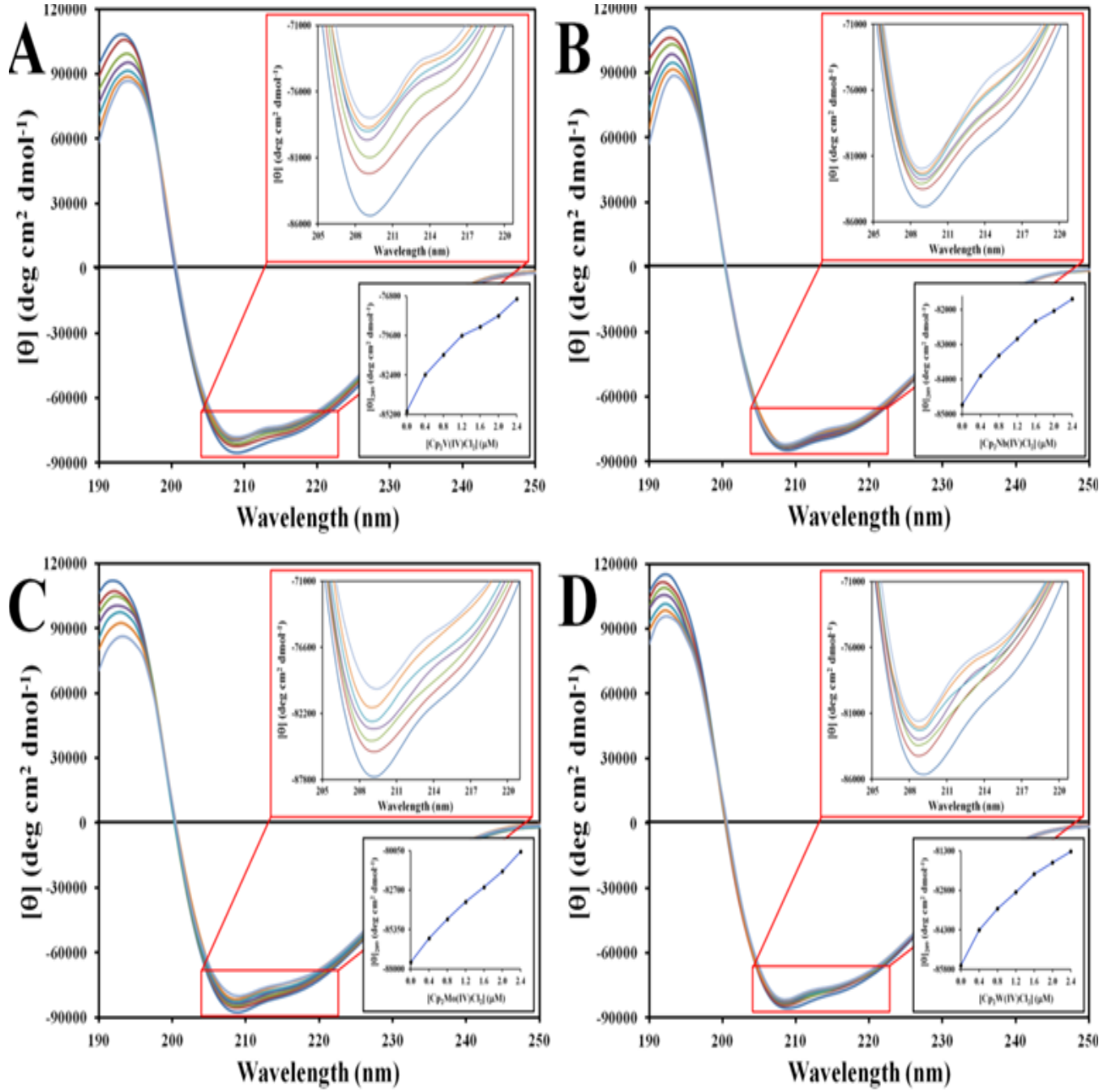

Figure 11 Far-UV CD spectra at 298 K of apo-hTf in 2.0 mM Tris-HCl, pH 7.4, in the presence and absence of Cp_2VCl_2 (A), Cp_2NbCl_2 (B), Cp_2MoCl_2 (C) and Cp_2WCl_2 (D). The red inset shows enlarged the region at 209 nm. The black inset shows a graph of the mean residue molar ellipticity [] at 209 nm vs [$Cp_2M(IV)Cl_2$].

Citation: Fernández JRG, Pita XN, Meléndez E, et al. Interaction of metallocene dichlorides with apo-human transferrin: A spectroscopic study and cytotoxic activity against human cancer cell lines. *Int J Mol Biol Open Access.* 2020;5(3):79–109. DOI: 10.15406/ijmboa.2020.05.00136

Copyright: ©2020 Fernández et al.

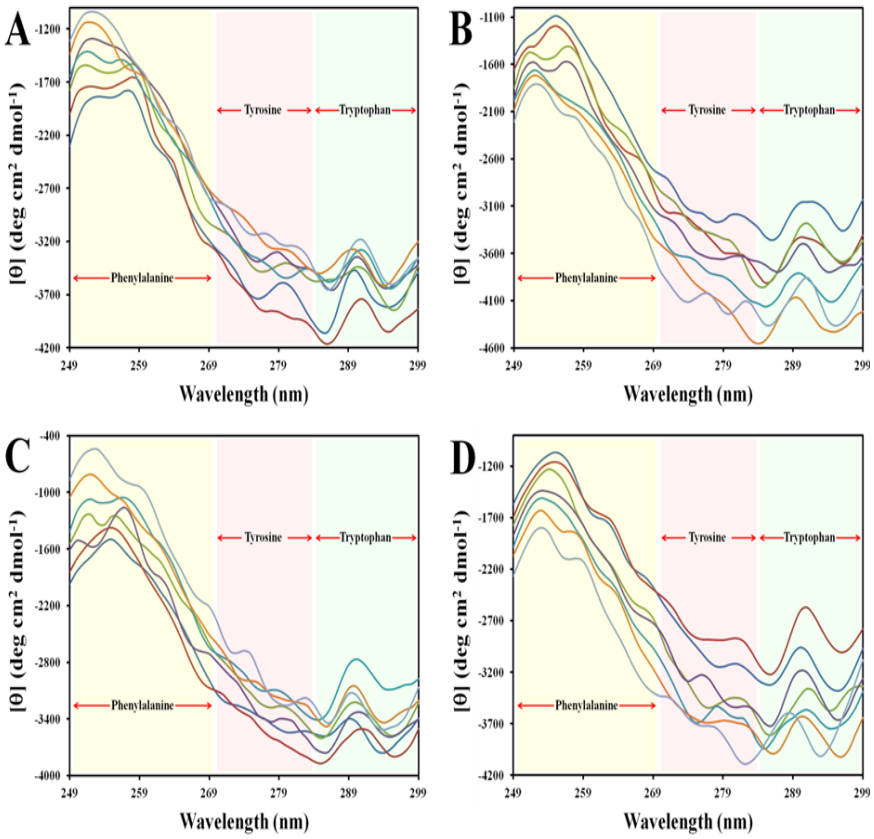

Figure 12 Near-UV CD spectra at 298 K of apo-hTf in 2.0 mM Tris-HCl, pH 7.4, in the absence and presence of Cp_2VCl_2 (A), Cp_2NbCl_2 (B), Cp_2MoCl_2 (C) and Cp_2WCl_2 (D).

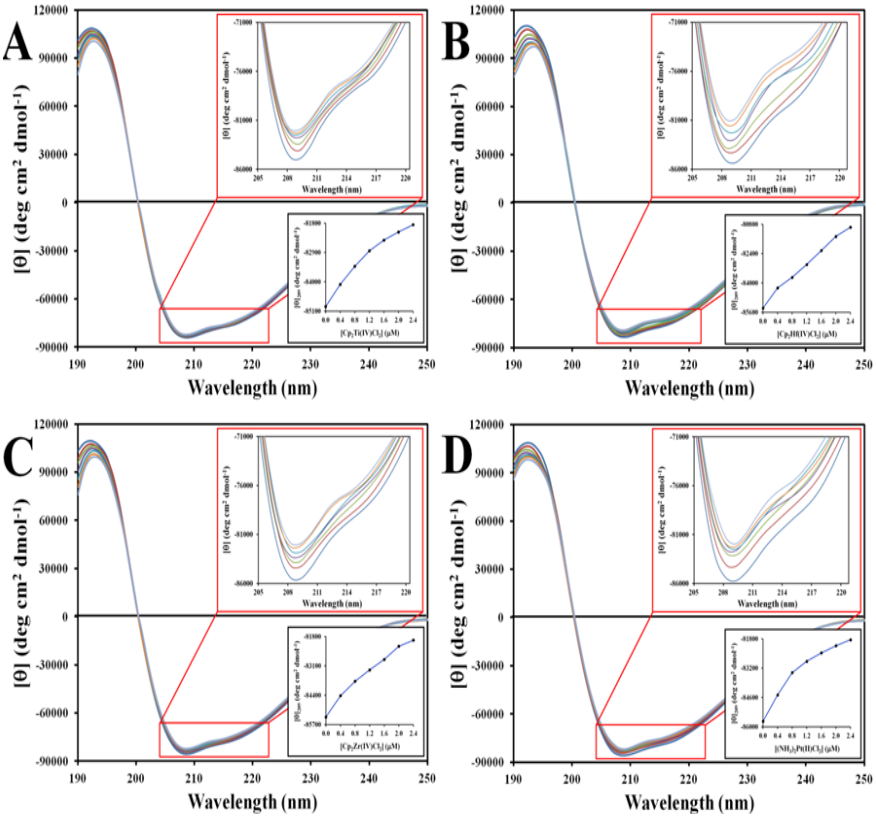

Figure S11 Far-UV CD spectra at 298 K of apo-hTf in 2.0 mM Tris-HCl, pH 7.4, in the absence and presenceof Cp_2TiCl_2 (A), Cp_2HfCl_2 (B), Cp_2ZrCl_2 (C) and $(NH_3)_2Pt(II)Cl_2$ (D). The red inset shows enlarged the region at 209 nm. The black inset shows a graph of the mean residue molar ellipticity [θ] at 209 nm vs $[Cp_2M(IV)Cl_2]$ or $[(NH_3)_2Pt(II)Cl_2]$.

Citation: Fernández JRG, Pita XN, Meléndez E, et al. Interaction of metallocene dichlorides with apo-human transferrin: A spectroscopic study and cytotoxic activity against human cancer cell lines. *Int J Mol Biol Open Access.* 2020;5(3):79–109. DOI: 10.15406/ijmboa.2020.05.00136

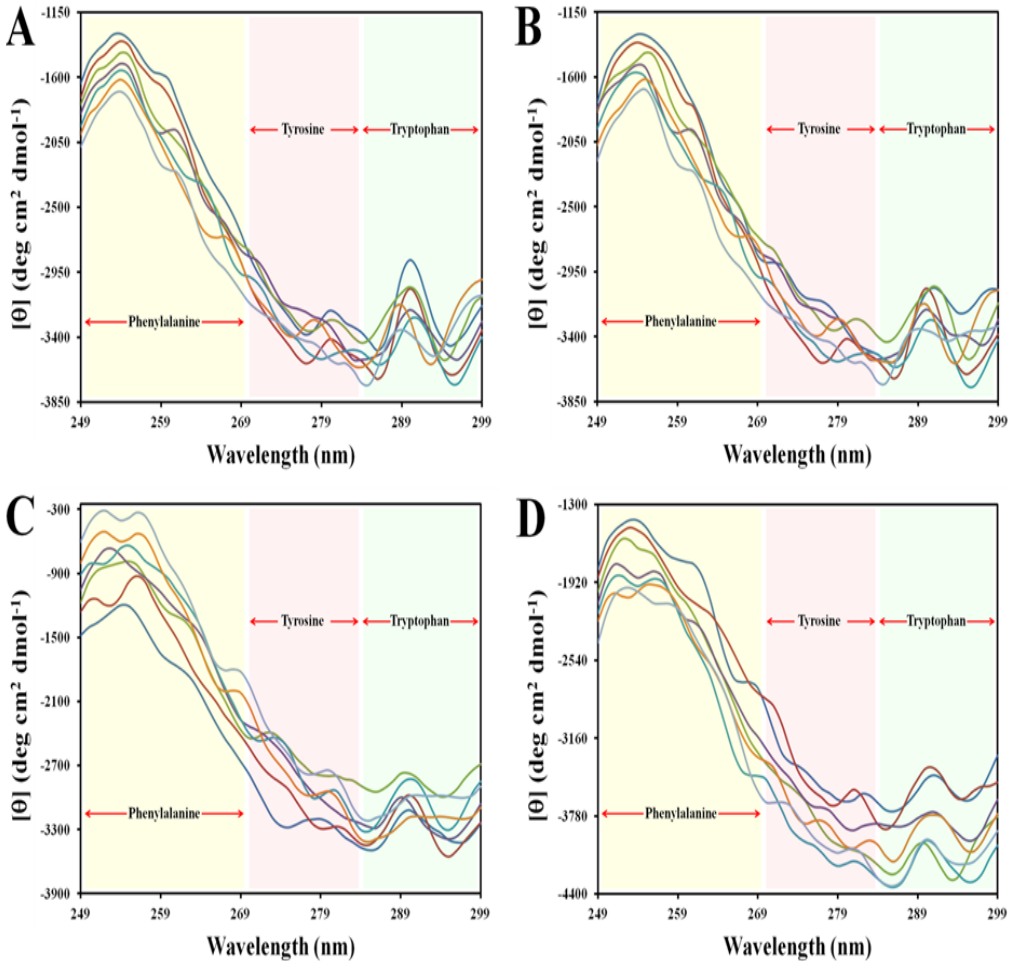

Figure S12 Near-UV CD spectra at 298 K of apo-hTf in 2.0 mM Tris-HCl, pH 7.4, in the absence and presence of Cp_2VCl_2 (A), Cp_2NbCl_2 (B), Cp_2MoCl_2 (C) and Cp_2WCl_2 (D).

Table 6 Contents secondary structure elements (α-helix, β-sheet, and random coil) of apo-hTf in the presence and absence of seven $Cp_2M(IV)Cl_2$ and DCCP based on the Raussens et al.'s method (CD-RRG)

Compound	Secondary structure elements	Contents secondary structure of apo-hTf (%)						
		Compound concentration (M)						
		0	0.4	0.8	1.2	1.6	2	2.4
Cp_2VCl_2	α-helix	29	28.4	27.9	27.2	26.5	25.8	25.1
	β-sheet	17.7	17.9	18.1	18.3	18.5	18.9	19.2
	random coil	33.5	33.7	33.9	34.1	34.3	34.5	34.6
	other	19.8	20	20.1	20.4	20.7	20.8	21.1
Cp_2NbCl_2	α-helix	29.8	29	28.7	27.6	26.9	26.2	25.4
	β-sheet	17.3	17.7	17.9	18.5	18.9	19	19.4
	random coil	33.6	33.8	34	34.2	34.4	34.6	34.8
	other	19.3	19.5	19.4	19.7	19.8	20.2	20.4
Cp_2MoCl_2	α-helix	29.3	28.7	28.3	27.6	27.1	26.5	25.8
	β-sheet	17.9	18.1	18.3	18.4	18.6	18.9	19.3
	random coil	33.8	33.9	34	34.1	34.3	34.5	34.7
	other	19	19.3	19.4	19.9	20	20.1	20.2

Table Continued....

Compound	Secondary structure elements	Contents secondary structure of apo-hTf (%)						
		Compound concentration (M)						
		0	0.4	0.8	1.2	1.6	2	2.4
Cp_2WCl_2	α-helix	30.2	29.8	29.5	29.1	28.3	27.9	27.5
	β-sheet	18.1	18.2	18.3	18.4	18.5	18.6	18.7
	random coil	33.5	33.7	33.8	33.9	34.1	34.3	34.4
	other	18.2	18.3	18.4	18.6	19.1	19.2	19.4
Cp_2TiCl_2	α-helix	29.5	29.3	29.1	29	28.8	28.6	28.4
	β-sheet	17.8	18	18.2	18.3	18.4	18.5	18.6
	random coil	33.8	33.8	33.8	33.9	33.9	34	34
	other	18.9	18.9	18.9	18.8	18.9	18.9	19
Cp_2HfCl_2	α-helix	29.8	29.7	29.5	29.3	29.1	29	28.7
	β-sheet	17.4	17.5	17.6	17.7	17.8	17.9	18
	random coil	33.6	33.7	33.8	33.8	34	34	34.1
	other	19.2	19.1	19.1	19.2	19.1	19.1	19.2
Cp_2ZrCl_2	α-helix	29.4	29.2	29.1	29	28.8	28.6	28.4
	β-sheet	18	18.1	18.2	18.3	18.4	18.5	18.6
	random coil	33.8	33.8	33.9	33.9	33.9	34	34.1
	other	18.8	18.9	18.8	18.8	18.9	18.9	18.9
$(NH_3)_2Pt(II)Cl_2$	α-helix	29.2	28.9	28.7	28.5	28.3	28.1	28
	β-sheet	18	18.1	18.2	18.3	18.4	18.5	18.6
	random coil	33.9	33.9	33.9	34	34	34.1	34.1
	other	18.9	19.1	19.2	19.2	19.3	19.3	19.3
Crystallographic or far-UV CD data reported by:		[96]	[109]	[108]				
apo-hTf	α-helix	31	32	41.5				
	β-sheet	18	22	28.4				
	random coil	51	46	30.1				
	other							

Perspective

This work put under perspective consistencies and discrepancies found in our preliminary *in silico* studies. The *in silico* studies helped us to explain how seven metallocene dichlorides [$Cp_2M(IV)Cl_2$ (M(IV) = Ti, Zr, Hf, V, Nb, Mo, W)] might be engaged in hydrophobic interactions with those amino acid residues located in the C-lobe or N-lobe of apo-hTf, outside of the iron binding site.[41] It is also shown that the stability of apo-hTf:$Cp_2M(IV)Cl_2$ complexes is in the order of V > Nb > Mo ~ W > Zr ~ Hf > Ti.[44] These results were consistent with experimental K_a and ΔG^o values, as shown in Tables 3&4, respectively. Furthermore, it seems that metallocene dichlorides are mainly engaged in hydrophobic and van der Waals interactions with apo-hTf, in correlation with the thermodynamic parameters ΔH^o and ΔS^o (Table 4). The van der Waals interaction became truly important for Ti, Zr and Hf, which mostly reveal their very low stability. The level of stability and binding affinity of $Cp_2M(IV)Cl_2$(M(IV) = Ti, Zr, Hf, V, Nb, Mo, W) also correlate to the type of quenching. Those metallocene dichlorides with very high binding affinity (M(IV) = V, Nb, Mo, W) can undergo static quenching, whereas those with low binding affinity (M(IV) = Ti, Zr, Hf) can undergo dynamic quenching. It is important to notice that their binding affinity also correlates to their CD titration spectra. Perturbations on secondary structures (α-helix, β-sheet and random coil) were more pronounced when of apo-hTf was titrated with $Cp_2M(IV)Cl_2$ (M(IV) = V, Nb, Mo, W). These four organometallic compounds have high binding affinity and are engaged in shorter distances with apo-hTf based on FNRET theory (Table 5). According to UV-Vis absorption analysis, titration of apo-hTf with $Cp_2M(IV)Cl_2$ (M(IV) = V, Mo, W) caused an immediate band formation at 361 nm attributed to MLCT, but this result was difficult to predict in our *in silico* studies because of the absence of water molecules. It is remarkable to notice this MLCT effect because the buffer under use does not have any synergistic anion to form a complex in the iron binding sites. Nevertheless, titration of $Cp_2M(IV)Cl_2$ (M(IV) = Mo and W) show that the band at 361 nm can appear after the fourth aliquot, suggesting that the first interaction of these two metallocene

dichlorides are mainly hydrophobic (in agreement with the *in silico* docking studies) and eventually they occupy a second binding site, most likely the iron binding site. Thus, the molecular mechanism of action forthe metallocene di chlorides (Figure 13) might involve accumulation in the nucleifollowed by alate step where coordination to DNA phosphates might occur for suppressing DNA synthesis and/or inhibition of nuclear enzymes,[44,46,49,53–55] while for cisplatin it is through an inter-strand crosslinked coordination of platinum to N7 of the guanine residue.[42,43,84] Based on our results, another possible mechanism mediated by apo-hTf might occur where $Cp_2M(IV)Cl_2$ (M(IV) = Ti, Zr, Hf, V, Nb, Mo, W) bind to different hydrophobic sites outside the iron binding sites. This new mode of interaction might abrogate the typical formation of the hTf:Tf-R (receptor) complex, thus suppressing the iron metabolism and transporting metallocene dichlorides inside the cell and, as a consequence, inducing cell death.

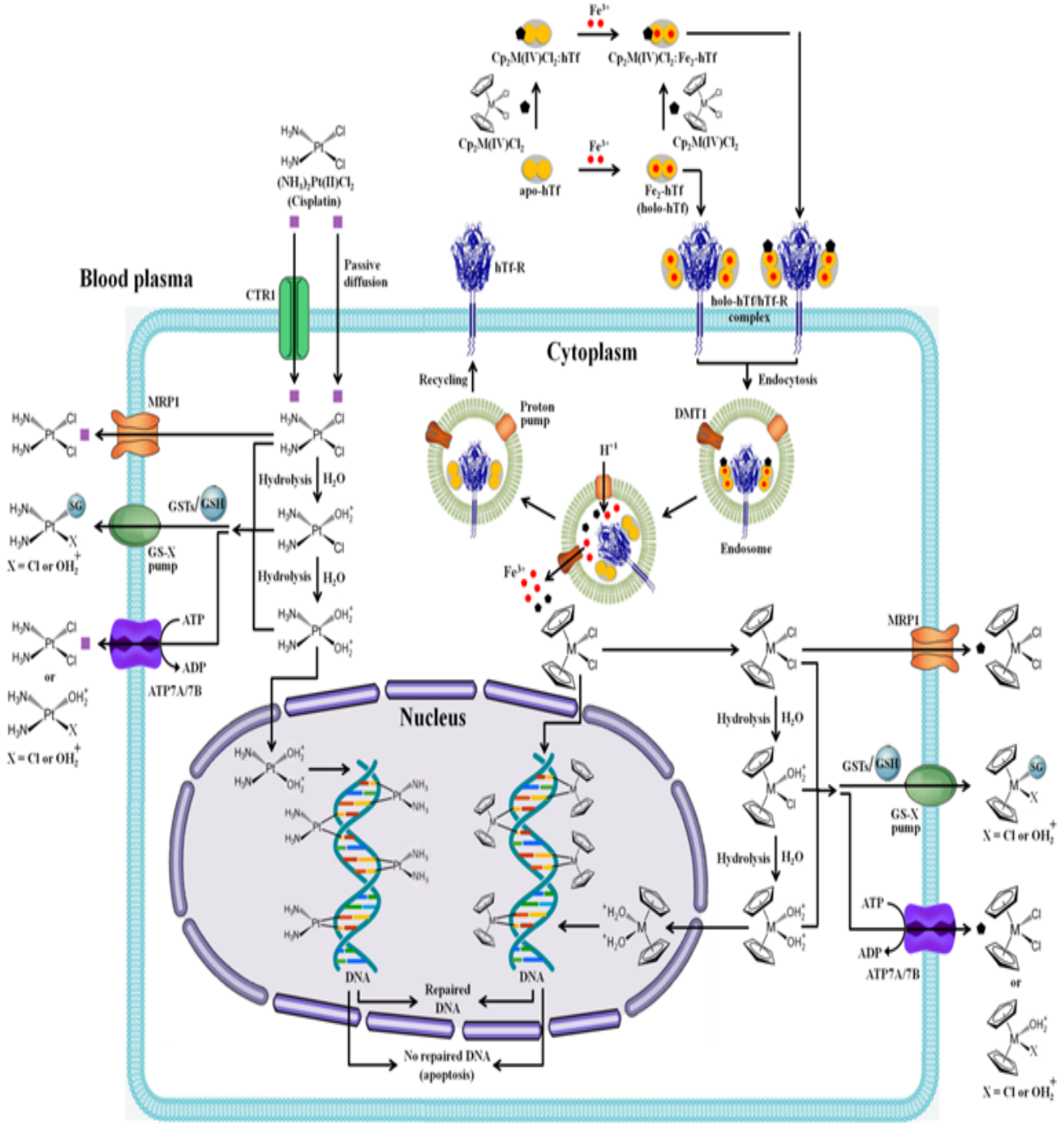

Figure 13 Proposed molecular mechanismof action for metallocene dichlorides ($Cp_2M(IV)Cl_2$) associated to the hTf:hTf-Rcomplex and for cisplatin ($(NH_3)_2Pt(II)Cl_2$).Abbreviations: CTR1 (chloride transport receptor 1); GSH (glutathione); GSTs (glutathione S-transferase); MRP1 (multidrug resistance-associated protein 1); GS-X pump (ATP-dependent glutathione S-conjugate export pump); ATP7A/7B (copper transporters ATPase copper-transporting alpha (ATP7A) and ATPase copper-transporting beta (ATP7B)).

Citation: Fernández JRG, Pita XN, Meléndez E, et al. Interaction of metallocene dichlorides with apo-human transferrin: A spectroscopic study and cytotoxic activity against human cancer cell lines. *Int J Mol Biol Open Access.* 2020;5(3):79–109. DOI: 10.15406/ijmboa.2020.05.00136

Conclusion

The cytotoxicity of several metallocene dichlorides against MCF-7 cells and HT-29 cells was determined using MTT assay, and their interaction with apo-hTf was investigated *in vitro* using different spectroscopic techniquesunder physiological conditions. All metallocene dichlorides exhibited an antiproliferative effect on HT-29 cells, whereas $Cp_2M(IV)Cl_2$ (M(IV) =V, Nb, Ti, W) and $Cp_2M(IV)Cl_2$ (M(IV) = Mo, Hf, Zr) exhibited an antiproliferative effect and proliferative activity on MCF-7 cells, respectively. Only Cp_2VCl_2 exhibited cytotoxicity similar to that of $(NH_3)_2Pt(II)Cl_2$ against both human cancer cell lines. Furthermore, apo-hTf has shown that can enhance the antiproliferative activity of $Cp_2M(IV)Cl_2$ (M(IV) = V, Nb and Mo), suggesting its vital role as a protein carrier of these three metallocene di chlorides. Changes in the UV-Vis absorption spectra also suggested formation of a ground state complex, and the CD data suggested that any interaction between a metallocene dichloride and apo-hTf could significantly affect the protein's conformation. Changes in secondary and tertiary structures became visible even at low concentration of these compounds. FRET results suggest that only three $Cp_2M(IV)Cl_2$ (M(IV) = V, Nb and Mo) has a strong binding affinity for apo-hTf by inducing a strong quenching effect on its fluorescence spectrum. Other metallocene dichlorides could bind this protein, but more weakly, maybe due to differences in their binding modes. Our study also showed that metallocene dichlorides quenched the apo-hTf intrinsic fluorescence mainly through a static quenching mechanism. Site binding constants and the number of binding sites for each protein-ligand complex formed were determined at four different temperatures. The calculated thermodynamic parameters suggest that hydrophobic forces are playing vital roles in their binding interaction, mainly through an endothermic and spontaneous process. Binding distances of these apo-hTf:$Cp_2M(IV)Cl_2$ complexes were calculated on the basis of the Forster's theory, which results suggest that the energy transfer could occur. Thus, all the experimental data have provided a valuable insight of the binding mechanism of $Cp_2M(IV)Cl_2$ for apo-hTf, in agreement with our previous *in silico* studies.

Acknowledgments

Dr. Enrique Meléndez is grateful for the financial support of NIH–COBRE II and NIHSCORE S06 GM008103–37 at UPR–Mayagüez. This publication was supported by an Institutional Development Award (IDeA) from the National Institute of General Medical Sciences of the National Institutes of Health under grant number P20 GM103475-14 and the RCMI grant U54 MD007600 (National Institute on Minority Health and Health Disparities) from the National Institutes of Health. The content is solely the responsibility of the authors and does not necessarily represent the official views of the National Institutes of Health.

Conflicts of interest

The authors declare that they have no conflicts of interest.

References

1. Köpf Maier P. Complexes of metals other than platinum as antitumour agents. *Eur J ClinPharmacol*. 1994;47(1):1–16.
2. Cranswick MA, Dawson A, Cooney JJA, et al. Photoelectron Spectroscopy and Electronic Structure Calculations of d1 Vanadocene Compounds with Chelated Dithiolate Ligands: Implications for Pyranopterin Mo/W Enzymes. *Inorg Chem*. 2007;46(25):10639–10646.
3. Gasser G, Ott I, Metzler-Nolte N. Organometallic anticancer compounds. *J Med Chem*. 2011;54(1):3–25.
4. Martins P, Marques M, Coito L, et al. Organometallic compounds in cancer therapy: past lessons and future directions. *Anticancer Agents Med Chem*. 2014;14(9):1199–1212.
5. Harding MM, Mokdsi G. Antitumour metallocenes: structure-activity studies and interactions with biomolecules. *Curr Med Chem*. 2000;7(12):1289–1303.
6. Pavlaki M, Debeli K, Triantaphyllidou IE, et al. A proposed mechanism for the inhibitory effect of the anticancer agent titanocene dichloride on tumour gelatinases and other proteolytic enzymes. *J Biol Inorg Chem*. 2009;14:947–957.
7. Shi Y, Harvey I, Campopiano D, et al. Niobium Uptake and Release by Bacterial Ferric Ion Binding Protein. *Bioinorg Chem Appl*. 2010;2010:1–11.
8. McLaughlin ML, Cronan JM, Schaller TR, et al. DNA Metal binding by antitumor-active metallocene dichlorides from inductively coupled plasma spectroscopy analysis: titanocene dichloride forms DNA-Cp_2Ti or DNA-CpTi adducts depending on pH. *J Am Chem Soc*.1990;112(24):8949–8952.
9. Köpf H, Köpf Maier P. Titanocene dichloride--the first metallocene with cancerostatic activity. *Angew Chem Int Ed Engl*. 1979;18(6):477–478.
10. Köpf Maier P, Köpf H. Vanadocen-dichlorid-einweiteres Antitumor-Agensaus der Metallocenreihe / Vanadocene Dichloride - Another Antitumor Agent from the Metallocene Series. *Z Naturforsch*. 1979;34b(6):805–807.
11. Köpf Maier P, Leitner M, Voigtlander R, et al. Molybdocene dichloride as an antitumor agent (author's transl). *Z Naturforsch*. 1979;34(12):1174–1176.
12. Köpf Maier P, Hesse B, Köpf H. Tumor inhibition by metallocenes: effect of titanocene, zirconocene, and hafnocene dichlorides on Ehrlich ascites tumor in mice (author's transl). *J Cancer Res Clin Oncol*. 1980;96(1):43–51.
13. Köpf Maier P, Leitner M, Köpf H. Tumor inhibition by metallocenes: antitumor activity of niobocene and tungstocene dichlorides. *J Inorg Nucl Chem*. 1980;42(12):1789–1791.
14. Köpf Maier P, Wagner W, Köpf H. *In vitro* cell growth inhibition by metallocene dichlorides. *Cancer Chemother Pharmacol*. 1981;5(4):237–241.
15. Köpf H, Köpf Maier P. Tumor Inhibition by Metallocene Dihalides of Early Transition Metals. *ACS Symp Ser*.1983;209:315–333.
16. Köpf Maier P, Wagner W, Hesse B, et al. Tumor inhibition by metallocenes: activity against leukemias and detection of the systemic effect. *Eur J Cancer*.1981;17(6):665–669.
17. Feliciano I, Matta J, Meléndez E. Water-soluble molybdenocene complexes with both proliferative and antiproliferative effects on cancer cell lines and their binding interactions with human serum albumin. *J Biol Inorg Chem*. 2009;14(7):1109–1117.
18. Gao LM, Meléndez E. Cytotoxic properties of titanocenyl amides on breast cancer cell line mcf-7. *Met Based Drugs*. 2010;2010:1–6.
19. Domínguez–García M, Ortega–Zúñiga C, Meléndez E. New tungstenocenes containing 3-hydroxy-4-pyrone ligands: antiproliferative activity on HT-29 and MCF-7 cell lines and binding to human serum albumin studied by fluorescence spectroscopy and molecular modeling methods. *J BiolInorg Chem*. 2013;18(2):195–209.
20. Hernández R, Lamboy J, Gao LM, et al. Structure-activity studies of Ti(IV) complexes: aqueous stability and cytotoxic properties in colon cancer HT-29 cells. *J BiolInorg Chem*. 2008;13(5):685–692.

21. Meléndez E. Bioorganometallic Chemistry of Molybdenocene Dichloride and Its Derivatives. *J Organomet Chem*. 2012;706–707:4–12.

22. Hernández R, Méndez J, Lamboy J, et al. Titanium(IV) complexes: cytotoxicity and cellular uptake of titanium(IV) complexes on caco-2 cell line. *Toxicol In Vitro*. 2010;24(1):178–183.

23. Ghosh P, D'Cruz OJ, Narla RK, et al. Apoptosis-inducing vanadocene compounds against human testicular cancer. *Clin Cancer Res*. 2000;6(4):1536–1545.

24. Köpf Maier P, Preiss F, Marx T, et al. Tumor inhibition by titanocene complexes: activity against sarcoma 180. *Anticancer Res*.1986;6(1):33–37.

25. Köpf Maier P, Köpf H. Tumor inhibition by titanocene complexes. Activity against B16 melanoma and colon 38 carcinoma. *Arzneimittelforschung*.1987;37(5):532–534.

26. Chang SI. Synthesis of metal compounds and experimental studies on the anti-tumor effects of substances from subgroup IV (translated from Chinese). *Yao Hsueh T'ung Pao*.1981;16:57.

27. Toney JH, Rao LN, Murthy MS, et al. *Breast Cancer Res Treat*. Ed. M. Nijhoff, The Hague, Boston, 1985;6:185.

28. Murthy MS, Toney JH, Rao LN, et al. *Proc Amer Assoc Cancer Res*.1986;27:279.

29. Goldin A, Wolpert-Defillippes MK. Nude mouse models as predictors of chemotherapy in man: thymidine and pyrimidines. *Bull Cancer*.1981;66(1):61–66.

30. Venditti JM. Preclinical drug development: rationale and methods. *Semin Oncol*.1981;8(4):349–361.

31. Köpf Maier P, Moormann A, Köpf H. Activity of titanocene dihalides against a human colon carcinoma heterotransplanted to athymic mice. *Eur J Chem Clin Oncol*.1985;21(7):853–857.

32. Köpf Maier P. Activity of metallocene complexes against human tumours heterotransplanted into athymic mice. In book: Human Tumour Xenografts in Anticancer Drug Development. Winograd B, Peckham MJ, Pinedo HM, Editors. ESO Monographs. Springer–Verlag, Berlin. 1987.

33. Köpf Maier P. Tumor inhibition by titanocene complexes: influence upon two xenografted human lung carcinomas. *J Cancer Res Clin Oncol*.1987;113:342–348.

34. Osieka R. Studies on drug resistance in a human melanoma xenograft system. *Cancer Treat Rev*.1984;11(Suppl A):85–98.

35. Köpf Maier P. Antitumor activity of titanocene dichloride in xenografted human renal-cell carcinoma. *Anticancer Res*.1999;19(1A):493–504.

36. Kopf Maier P, Kopf H. Metallocene complexes: organometallic antitumor agents. *Drugs Future*.1986;11:297–320.

37. Clearfield A, Warner DK, Saldarriaga Molina CH, et al. Structural Studies of $(\pi\text{-}C_5H_5)_2MX_2$ Complexes and their Derivatives. The Structure of Bis(π-cyclopentadienyl)titanium Dichloride. *Can J Chem*.1975;53(11):1622–1629.

38. Cranswick MA, Gruhn NE, Enemark JH, et al. Electronic Structure of the d^1 Bent Metallocene Cp_2VCl_2: A Photoelectron and Density Functional Study. *J Organomet Chem*.2008;693(8-9):1621–1627.

39. Prout K, Cameron TS, Forder RA, et al. The crystal and molecular structures of bent bis-π-cyclopentadienyl Metal complexes: (a) bis-π-cyclopentadienyldibromorhenium(V) tetrafluoroborate, (b) bis-π-cyclopentadienyldichloromolybdenum(IV), (c) bis-π-cyclopentadienylhydroxomethylaminomolybdenum(IV) hexafluorophosphate, (d) bis-π-cyclopentadienylethylchloromolybdenum(IV), (e) bis-π-cyclopentadienyldichloroniobium(IV), (f) bis-π-cyclopentadienyldichloromolybdenum(V) tetrafluoroborate, (g) μ-oxo-bis[bis-π-cyclopentadienylchloroniobium(IV)] tetrafluoroborate, (h) bis-π-cyclopentadienyldichlorozirconium. *Acta Cryst*.1974;B30:2290–2304.

40. Suárez D, Zakarianezhad M, López R. Insights into the hydrolytic chemistry of molybdocene dichloride based on a theoretical mechanistic study. *Theor Chem Acc*. 2013;132:1409–1419.

41. Güette-Fernández JR, Meléndez E, Maldonado-Rojas W, et al. A molecular docking study of the interactions between human transferrin and seven metallocene dichlorides. *J Mol Graph Model*.2017;75:250–265.

42. Milburn GHM, Truter MR. The crystal structures of cis- and trans-dichlorodiammineplatinum(II). *J Chem Soc A*.1966;11:1609–1616.

43. Ting VP, Schmidtmann M, Wilson CC, et al. Cisplatin: polymorphism and structural insights into an important chemotherapeutic drug. *Angew Chem Int Ed Engl*. 2010;49(49):9408–9411.

44. Köpf Maier P, Krahl D. Tumor inhibition by metallocenes: ultrastructural localization of titanium and vanadium in treated tumor cells by electron energy loss spectroscopy. *Chem Biol Interact*.1983;44(3):317–328.

45. Köpf Maier P. Intracellular localization of titanium within xenografted sensitive human tumors after treatment with the antitumor agent titanocene dichloride. *J Struct Biol*. 1990;105(1-3):35–45.

46. Waern JB, Harris HH, Lai B, et al. Intracellular mapping of the distribution of metals derived from the antitumor metallocenes. *J Biol Inorg Chem*. 2005;10(5):443–452.

47. Köpf Maier P, Köpf H. Tumor inhibition by titanocene dichloride: first clues to the mechanism of action. *Naturwissenschaften*.1980;67(8):415–416.

48. Murthy MS, Rao LN, Kuo LY, et al. Antitumor and toxicologic properties of the organometallic anticancer agent vanadocene dichloride. *Inorg Chim Acta*.1988;152(2):117–124.

49. Murray JH, Harding MM. Organometallic anticancer agents: the effect of the central metal and halide ligands on the interaction of metallocene dihalides Cp_2MX_2 with nucleic acid constituents. *J Med Chem*.1994;37(13):1936–1941.

50. Kuo LY, Kanatzidis MG, Sabat M, et al. Metallocene antitumor agents. Solution and solid-state molybdenocene coordination chemistry of DNA constituents. *J Am Chem Soc*. 1991;113(24):9027–9045.

51. Köpf Maier P, Köpf H. Transition and main-group metal cyclopentadienyl complexes: preclinical studies on a series of antitumor agents of different structural type. *Bioinorg Chem. Part of Struct Bond*. 2005;70:103–185.

52. Köpf Maier P. *Dev Oncol*.1988;54:601.

53. Köpf Maier P, Wagner W, Köpf H. Different inhibition pattern of the nucleic acid metabolism after in vitro treatment with titanocene and vanadocene dichlorides. *Naturwissenschaften*. 1981;68(5):272–273.

54. Köpf Maier P, Krahl D. Intracellular distribution of titanium after treatment with the antitumor agent titanocene dichloride: on electron energy loss spectroscopic study. *Naturwissenschaften*.1981;68(5):273–274.

55. Kuo LY, Liu AH, Marks TJ. Metallocene interactions with DNA and DNA-processing enzymes. *Met Ions Biol Syst*. 1996;33:53–85.

56. Sudquist WI, Lippard SJ. The coordination chemistry of platinum anticancer drugs and related compounds with DNA. *Coord Chem Rev*. 1990;100:293–322.

57. Harding MM, Harden GJ, Field LD. A 31P NMR study of the interaction of the antitumor active metallocene Cp_2MoCl_2 with calf thymus DNA. *FEBS Lett*. 1993;322(3):291–294.

58. Toney JH, Brock CP, Marks TJ. Aqueous coordination chemistry of vanadocene dichloride with nucleotides and phosphoesters. Mechanistic implications for a new class of antitumor agents. *J Am Chem Soc*. 1986;108(23):7263–7274.

59. Christodoulou CV, Ferry DR, Fyfe DW, et al. Phase I trial of weekly scheduling and pharmacokinetics of titanocene dichloride in patients with advanced cancer. *J Clin Oncol*. 1998;16(8):2761–2769.

60. Korfel A, Scheulen ME, Schmoll HJ, et al. Phase I clinical and pharmacokinetic study of titanocene dichloride in adults with advanced solid tumors. *Clin Cancer Res*. 1998;4(11):2701–2708.

61. Lummen G, Sperling H, Luboldt H, et al. Phase II trial of titanocene dichloride in advanced renal-cell carcinoma. *Cancer ChemotherPharmacol*. 1998;42(5):415–417.

62. Kröger N, Kleeberg UR, Mross K, et al. Phase II Clinical Trial of Titanocene Dichloride in Patients with Metastatic Breast Cancer. *Onkologie*. 2000;23:60–62.

63. Du H, Xiang J, Zhang Y, et al. Binding of V(IV) to human transferrin: potential relevance to anticancer activity of vanadocene dichloride. *J InorgBiochem*. 2008;102(1):146–149.

64. Zhang Y, Xiang J, Liu Y, et al. Constructing transferrin receptor targeted drug delivery syst*em by using doxorubi*cin hydrochloride and vanadocene dichloride. *Bioorg Med Chem Lett*. 2011;21(19):5982–598.

65. Domínguez M, Cortés Figueroa JE, Meléndez E. Biological Interaction of Molybdenocene Dichloride with Bovine Serum Albumin Using Fluorescence Spectroscopy. *J Chem Educ*. 2018;95(1):152–157.

66. Sarsam SW, Nutt DR, Strohfeldt K, et al. Titanocene anticancer complexes and their binding mode of action to human serum albumin: a computational study. *Metallomics*. 2011;3(2):152–161.

67. Mokdsi G, Harding MM. Inhibition of human topoisomerase II by the antitumor metallocenes. *J InorgBiochem*. 2001;83(2-3):205–209.

68. Narváez Pita X, Ortega Zúñiga C, Acevedo Morantes CY, et al. Water soluble molybdenocene complexes: synthesis, cytotoxic activity and binding studies to ubiquitin by fluorescence spectroscopy, circular dichroism and molecular modeling. *J InorgBiochem*. 2014;132:77–91.

69. Luck AN, Mason AB. Transferrin Mediated cellular iron delivery. *Curr Top Membr*. 2012;69:3–35.

70. Buddanavar AT, Nandibewoor ST. Multi-spectroscopic characterization of bovine serum albumin upon interaction with atomoxetine. *J Pharm Anal*. 2017;7(3):148–155.

71. Wang R, Liu Y, Hu X, et al. New insights into the binding mechanism between osthole and β-lactoglobulin: Spectroscopic, chemometrics and docking studies. *Food Res Int*. 2019;120:226–234.

72. Heller GT, Aprile FA, Vendruscolo M. Methods of probing the interactions between small molecules and disordered proteins. *Cell Mol Life Sci*. 2017;74(17):3225–3243.

73. Bull SC, Doig AJ. Properties of protein drug target classes. *PLoSOne*. 2015;10(3):0117955.

74. de Juan A, Rutan SC, Tauler R, et al. Comparison between the direct trilinear decomposition and the multivariate curve resolution-alternating least-squares methods for the resolution of 3-way data sets. *Chemom Intell Lab Sys*. 1998;40(1):19–32.

75. Cheng Z, Liu R, Jiang X. Spectroscopic studies on the interaction between tetrandrine and two serum albumins by chemometrics methods. *SpectrochimActa A Mol BiomolSpectrosc*. 2013;115:92–105.

76. Li H, Sun H, Qian ZM. The role of the transferrin-transferrin-receptor system in drug delivery and targeting. *Trends Pharmacol Sci*. 2002;23(5):206–209.

77. Narváez Pita X, Rheingold AL, Meléndez E. Ferrocene-steroid conjugates: Synthesis, structure and biological activity. *J Organomet Chem*. 2017;846:113–120.

78. Pérez Y, López V, Rivera Rivera L, et al. Water-soluble titanocene complexes with sulfur-containing amino acids: synthesis, spectroscopic, electrochemical and Ti(IV)-transferrin interaction studies. *J BiolInorg Chem*. 2005;10(2):94–104.

79. Lakowicz JR. *Principles of Fluorescence Spectroscopy*, 3rd ed. Springer, New York. 2006.

80. Mossman T. Rapid colorimetric assay for cellular growth and survival: application to proliferation and cytotoxicity assays. *J Immunol Methods*. 1983;65(1–2):55–63.

81. Denizot F, Lang R. Rapid colorimetric assay for cell growth and survival. Modifications to the tetrazolium dye procedure giving improved sensitivity and reliability. *J Immunol Methods*. 1986;89(2):271–277.

82. Meléndez E. Metallocenes as Target Specific Drugs for Cancer Treatment. *Inorganica ChimActa*. 2012;393:36–52.

83. Schäfer S, Ott I, Gust R, et al. Influence of the Polypyridyl (pp) Ligand Size on the DNA Binding Properties, Cytotoxicity and Cellular Uptake of Organoruthenium(II) Complexes of the Type $[(\eta^6\text{-}C_6Me_6)Ru(L)(pp)]^{n+}$ [L=Cl, n=1; L=$(NH_2)_2$CS, n=2]. *Eur J Inorg Chem*. 2007;2007(19):3034–3046.

84. Mizumura Y, Matsumura Y, Hamaguchi T, et al. Cisplatin-incorporated polymeric micelles eliminate nephrotoxicity, while maintaining antitumor activity. *Jpn J Cancer Res*. 2001;92(3):328–336.

85. Leong KH, Looi CY, Loong XM, et al. Cycloart-24-ene-26-ol-3-one, a New Cycloartane Isolated from Leaves of Aglaia exima Triggers Tumour Necrosis Factor-Receptor 1 Mediated Caspase-Dependent Apoptosis in Colon Cancer Cell Line. *PLoS One*. 2016;11(4):e0152652.

86. Feliciano I, Matta J, Melendez E. Water-soluble molybdenocene complexes with both proliferative and antiproliferative effects on cancer cell lines and their binding interactions with human serum albumin. *J BiolInorg Chem*. 2009;14(7):1109–1117.

87. Kuo LY, Kanatzidis MG, Sabat M, et al. Metallocene antitumor agents. Solution and solid-state molybdenocene coordination chemistry of DNA constituents. *J Am Chem Soc*. 1991;113(24):9027–9045.

88. Toney JH, Marks TJ. Hydrolysis chemistry of the metallocene dichlorides $M(\eta^5\text{-}C_5H_5)_2Cl_2$, M=titanium, vanadium, or zirconium. Aqueous kinetics, equilibria, and mechanistic implications for a new class of antitumor agents. *J Am Chem Soc*. 1985;107(4):947–953.

89. Köpf H, Köpf Maier P. Chemistry and Biochemistry. In: SJ Lippard, Editor. Platinum, Gold, and Other Metal Chemotherapeutic Agents, Chapter 16:315–333.1983.

90. Chen T, Zhu S, Cao H, et al. Studies on the interaction of salvianolic acid B with human hemoglobin by multi-spectroscopic techniques. *SpectrochimActa A Mol BiomolSpectrosc*. 2011;78(4):1295–1301.

91. Pan X, Qin P, Liu R, et al. Characterizing the Interaction between tartrazine and two serum albumins by a hybrid spectroscopic approach. *J Agric Food Chem*. 2011;59(12):6650–6656.

92. Sahoo BK, Ghosh KS, Dasgupta S. Molecular interactions of isoxazolcurcumin with human serum albumin: spectroscopic and molecular modeling studies. *Biopolymers*. 2009;91(2):108–119.

93. Patel BK, Dasmandal S, Mahapatra A. Unraveling the binding of phenolphthalein with serum protein and releasing by β-cyclodextrin. *J Mol Liq*. 2017;244:330–339.

94. Buddanavar AT, Nandibewoor ST. Multi-spectroscopic characterization of bovine serum albumin upon interaction with atomoxetine. *J Pharm Anal*. 2017;7(3):148–155.

95. Suryawanshi VD, Walekar LS, Gore AH, et al. Spectroscopic analysis on the binding interaction of biologically active pyrimidine derivative with bovine serum albumin. *J Pharm Anal*. 2016;6(1):56–63.

96. Karimian Amroabadi M, Taheri Kafrani A, Heidarpoor Saremi L, et al. Spectroscopic studies of the interaction between alprazolam and apo-human serum transferrin as a drug carrier protein. *Int J BiolMacromol*. 2018;108:263–271.

97. Stephanos JJ, Farina SA, Addison AW. Iron ligand recognition by monomeric hemoglobins. *Biochim Biophys Acta*. 1996;1295(2):209–221.

98. Enyedy EA, Dömötör O, Bali K, et al. Interaction of the anticancer gallium(III) complexes of 8-hydroxyquinoline and maltol with human serum proteins. *J Biol Inorg Chem*. 2015;20(1):77–88.

99. Sulkowska A. Interaction of drugs with bovine and human serum albumin. *J Mol Struct*. 2002;614(1–3):227–232.

100. Dufour C, Dangles O. Flavonoid-serum albumin complexation: determination of binding constants and binding sites by fluorescence spectroscopy. *Biochim Biophys Acta*. 2005;1721(1–3):164–173.

101. Ross PD, Subramanian S. Thermodynamics of protein association reactions: forces contributing to stability. *Biochemistry*. 1981;20(11):3096–3102.

102. Sinanoglu O. *Modern quantum chemistry. First Edition*. Academic Press, New York. 1965.

103. Roy S, Nandi RK, Ganai S, et al. Binding interaction of phosphorus heterocycles with bovine serum albumin: A biochemical study. *J Pharm Anal*. 2017;7(1):19–26.

104. Preus S, Kilsa K, Miannay FA, et al. FRETmatrix: a general methodology for the simulation and analysis of FRET in nucleic acids. *Nucleic Acids Res*. 2013;41(1):18.

105. Sarzehi S, Chamani J. Investigation on the interaction between tamoxifen and human holo-transferrin: determination of the binding mechanism by flüüuorescence quenching, resonance light scattering and circular dichroism methods. *Int J BiolMacromol*. 2010;47(4):558–569.

106. Raussens V, Ruysschaert JM, Goormaghtigh E. Protein concentration is not an absolute prerequisite for the determination of secondary structure from circular dichroism spectra: a new scaling method. *Anal Biochem*. 2003;319(1):114–121.

107. Tomimatsu Y, Vickery LE. Circular dichroism studies of human serum transferrin and chicken ovotransferrin and their copper complexes. *Biochim Biophys Acta*. 1972;285(1):72–83.

108. Ali SA, Joao HC, Csonga R, et al. High-yield production of functionally active human serum transferrin using a baculovirus expression system, and its structural characterization. *Biochem J*. 1996;319(Pt 1):191–195.

109. Anderson BF, Baker HM, Dodson EJ, et al. Structure of human lactoferrin at 3.2-A resolution. *Proc NatiAcad Sci*. 1987;84(7):1769–1773.